

**ADHESION MECHANICS AND PHYSICAL CHARACTERISTICS OF *SALMONELLA*  
ENTERITIDIS IN LOW MOISTURE ENVIRONMENTS**

By

Quincy Jerome Suehr

A THESIS

Submitted to  
Michigan State University  
in partial fulfillment of the requirements  
for the degree of

Biosystems Engineering – Master of Science

2020

## ABSTRACT

### ADHESION MECHANICS AND PHYSICAL CHARACTERISTICS OF *SALMONELLA* ENTERITIDIS IN LOW MOISTURE ENVIRONMENTS

By

Quincy Jerome Suehr

Controlling foodborne pathogens in low-moisture environments requires an understanding of how contamination is introduced and spread through a system. Compared with numerous data and studies regarding wet environments, limited information exists concerning the adhesion mechanics of pathogens in low-moisture environments. Therefore, the objectives of this study were to: (1) Develop a framework for adhesion of bacteria in a low moisture environment, (2) perform direct measurements of adhesion mechanics, (3) implement measurements into a model, and (4) validate the model. Physical properties and adhesion characteristics of *Salmonella* Enteritidis PT30 (SE PT30) attached on stainless steel 304 were assessed by Atomic Force Microscopy (AFM) and Scanning Electron Microscopy (SEM), and used to develop a Discrete Element Method (DEM) model as a first principle based approach. This model allowed the estimation of force of reversible adhesion for *Salmonella* Enteritidis PT30 to be measured as  $F_{ad} = 3.3459 \pm 0.0283$  nN. For model validation, a large-scale bacterial detachment experiment utilizing *Salmonella* was conducted. The modeling results for adhesion was able to elucidate bacterial adhesion mechanics, and the cross-contamination phenomena in low-moisture environment.

Copyright by  
QUINCY JEROME SUEHR  
2020

## ACKNOWLEDGEMENTS

I would like to express my sincerest gratitude to Dr. Sanghyup Jeong, my major advisor, teacher, and friend. His continual guidance and mentorship from my undergraduate years to this thesis has truly helped me fully understand what it means to be a scientist, engineer, and leader.

Grateful appreciation is extended to guidance committee members Dr. Bradley Marks, Dr. Elliot Ryser, and Dr. Kirk Dolan, each individually providing expertise and direction in how to approach portions of this investigation. A special thanks to the Michigan State University Food Safety Engineering research team graduate students, undergraduates, and lab managers Mike James and Nicole Hall. Without everyone's support and hard work in the lab, none of this would be possible. Team TRIOPS consisting of: Dr. Sanghyup Jeong, Joanna Carrol, Phil Steinbrunner, and Chris Wells deserve recognition for the constant quest for 'moonshot ideas' in food safety.

Finally, thank you to my mother and father, for their constant support, my sister and brother-in-law's discussion times across many topics. Their involvement truly helped me understand the more important aspects of life, providing balance and energy to accomplish.

The author is indebted to the United States Department of Agriculture (USDA) Agriculture and Food Research Initiative (AFRI) for supporting grant 2013-67017-21227 titled "Understanding Bacterial Dry Transfer Mechanism during Nut Processing", which this study is a part of.

# TABLE OF CONTENTS

LIST OF TABLES .....	vii
LIST OF FIGURES .....	viii
CHAPTER 1. INTRODUCTION .....	1
1.1 Background .....	1
1.1.1 Statistics for Foodborne Illnesses .....	1
1.1.2 Low-Moisture Food Safety .....	1
1.1.3 Why Cross-Contamination Matters .....	3
1.2 Pertinent Literature Review .....	5
1.2.1 Previous Approach.....	5
1.2.2 New Approach .....	5
1.3 Objectives.....	7
CHAPTER 2. THEORIES .....	8
2.1 Adhesion Theories.....	8
2.1.1 Background Knowledge.....	8
2.1.2 JKR Cohesion for Particulates and Granular Physics.....	13
2.1.3 Adhesion Measurement Techniques .....	16
2.2 DEM Modeling .....	18
CHAPTER 3. METHODS AND PROCEDURES .....	20
3.1 Overall Approach .....	20
3.2 Mass of Bacteria.....	21
3.3 Size and Shape of Bacteria.....	23
3.4 Direct Measurement for Bacteria and Surface Characterization Using AFM .....	25
3.5 Statistical Quantification Using Centrifuge .....	27
3.5.1 Inoculation and Sample Preparation .....	27
3.6 First Principle Based DEM Modeling.....	29
3.7 Monte Carlo Modeling.....	29
CHAPTER 4. RESULTS AND DISCUSSION .....	31
4.1 Experimental Results.....	31
4.1.1 Mass distribution of SEPT30 for modeling .....	31
4.1.2 SEM Imaging and Size Distribution Based upon Images.....	31
4.1.3 AFM Imaging and Force Measurements .....	35
4.1.4 Centrifuge Experiment Results .....	42
4.2 DEM Modeling .....	45
4.2.1 DEM Modeling and Visualization .....	45
4.2.2 Monte Carlo Modeling Based upon Fundamental Properties.....	47
4.3 Summary .....	48
4.4 Discussion .....	49
CHAPTER 5. CONCLUSIONS .....	51

5.1	First Principle Based Modeling.....	51
5.2	Suggestions.....	51
APPENDICES .....		53
APPENDIX A. Scanning Electron Microscopy Images .....		54
APPENDIX B. Atomic Force Microscopy Data.....		57
APPENDIX C. Modeling Code .....		58
BIBLIOGRAPHY.....		65

## LIST OF TABLES

Table 1 Mean and confidence interval values of the major axis, minor axis, and circularity of elliptical shape approximation for <i>Salmonella</i> Enteritidis PT30 on stainless steel surface.....	34
Table 2 Root Mean Squared (RMS) surface roughness for each stainless steel finish type.....	36
Table 3 Cypher AFM calculated Young's modulus and JKR contact area of desiccated <i>Salmonella</i> Enteritidis PT30 on stainless steel surface.....	42

## LIST OF FIGURES

Figure 1 Almond harvesting process that sweeps dried almonds on the ground (courtesy of www.almond.com)..... 4

Figure 2 Interaction of a bacterial cell with a solid surface (Araújo, et al., 2009). ..... 9

Figure 3 DLVO Interaction energy of colloids interacting in an aqueous solution, showing the Double-Layer Repulsion (blue dotted line), and the van der Waals attraction (red dotted line) limits, and the competition between the two forces (black lines), in dimensionless units (Israelachvili, 2011). ..... 11

Figure 4 Contact angle between a surface and the liquid, can be used to calculate the surface energy level ( $\gamma$ ) of the microbes in the liquid solution (Israelachvili, 2011). ..... 13

Figure 5 Comparison of JKR theory for: A a rigid sphere, B. a deformed sphere from a downward force, and C. a positive force and resistance to detachment by the surface energy, consistent with the JKR theory (Israelachvili, 2011). ..... 15

Figure 6 Determination of adhesion force, where a sample is held in the centrifuge vial and is detached in the normal direction of the force as the sample rotates (You & Wan, 2014). ..... 17

Figure 7 Overall approach for acquisition of individual bacterial measurements, application of results to a first principle based DEM model, and explanation of the large scale canonical experiments using Monte Carlo modeling ..... 21

Figure 8 Optical microscope image of Au coated tip-less PNP AFM cantilever and a dense population of bacteria on the surface. The tip-less cantilever was used to measure adhesion force on bacteria. .... 27

Figure 9 Stainless steel 304 #4 brushed (left) #8 mirror finish (right) coupons used in the centrifuge experiment for measuring critical attachment force of *Salmonella* Enteritidis PT30 in a low-moisture environment. .... 28

Figure 10 Centrifuge sample holder (left) inserted in centrifuge tube (right) used for a centrifuge block (SS-34). Fabricated in the Department of Biosystems and Agricultural Engineering Shop, Michigan State University (East Lansing, MI). ..... 28

Figure 11 *Salmonella* Enteritidis PT30 mass measurements from methods described in Section 3.2 (avg mass = 1.19 pg and SD = 0.248 pg). ..... 31

Figure 12 Original SEM image of *Salmonella* Enteritidis PT30 on stainless steel (304 #4 brushed finish) (left) and the processed image (right) using ImageJ, where the cells can be identified from the background for further image analysis. .... 32

Figure 13 The distribution of the major and minor axis dimensions of <i>Salmonella</i> Enteritidis PT30 attached and desiccated on the surface of stainless steel. ....	33
Figure 14 The distribution of the circularity (ellipsoid approximation) of <i>Salmonella</i> Enteritidis PT30 attached and desiccated on the surface of stainless steel. ....	34
Figure 15 Optical microscope image of the Cypher AFM performing topographical measurements of the stainless steel #4 brushed finish using a 300kHz SiN tip. ....	35
Figure 16 AFM Alternating Current (AC) topographical visualizations of stainless steel finishes #4 (left) and #8 Mirror (right), demonstrating a noticeable difference in surface roughness.....	36
Figure 17 Height retrace from AFM of stainless steel 304 #4 brushed (left) and #8 Mirror (right) to determine the average surface roughness (RMS). ....	37
Figure 18 AFM image of desiccated a <i>Salmonella</i> cell on stainless steel #8 finish (AC Topographical mode of Cypher AFM with 300 kHz Silicon Nitride (SiN) fine point tip). ....	38
Figure 19 Force Mapping of <i>Salmonella</i> and stainless steel showing high force areas (white) are where bacteria is located, low force areas (black) is the surface, where little interaction occurs.	39
Figure 20 Interaction force between stainless steel and cantilever (A.), and the <i>Salmonella</i> and the cantilever (B.). Retraction from the surface is deflected based on the adhesion force interacting with the cantilever and the surface. ....	39
Figure 21 Histogram of maximum adhesion force from AFM force mapping of cantilever-surface (near zero points) and cantilever- <i>Salmonella</i> (~>3.0 nN). ....	40
Figure 22 Histogram of maximum adhesion forces for: (A) <i>Salmonella</i> interacting with a stainless steel surface; (B) <i>Salmonella</i> attached to a cantilever interacting with <i>Salmonella</i> on stainless steel surface. ....	41
Figure 23 Critical attachment force measurements for <i>Salmonella</i> Enteritidis PT30 attached on stainless steel coupons (#4, and #8 finish), the positive (control, 0 RPM) and the samples centrifuged at 5000 RPM (treated, 5000 RPM). ....	44
Figure 24 The remaining population (Log(CFU/cm <sup>2</sup> )) of desiccated <i>Salmonella</i> Enteritidis PT30 attached to stainless steel (#8 finish) after centrifugation at 300, 1000, 4000, 5000, and 10000 RPM. ....	45
Figure 25 Detachment of the multi-spherical model bacterium from the surface with an increasing pull off force in the +Z direction (upward). ....	46
Figure 26 Integer number of model bacteria remaining attached to a surface as a linear increase of detachment force.....	47

Figure 27 Experimental data (blue diamond symbol) vs. Monte Carlo modeling data (red cross symbol) for attachment force (via centrifugal force) distribution of *Salmonella* Enteritidis PT30 to stainless steel surface in low-moisture environment. .... 48

Figure 28 Initial moisture ring observed around the individualized *Salmonella* Enteritidis PT30 on stainless steel from SEM imaging..... 54

Figure 29 Conglomerates of *Salmonella* Enteritidis PT 30 harbor around grooves of the metal, #4 surface finish, increasing contact area with surface, significantly increasing the amount of force required to remove the bacteria..... 55

Figure 30 High concentrations of *Salmonella* deposited on the surface of stainless steel creates a dense multiple layer environment for the bacteria, indicating that initial concentration of bacteria directly effects the contact area and surface energy associated with adhesion of bacteria..... 55

Figure 31 Remnants of the flagella and ECM from *Salmonella* Enteritidis PT30 can still survive the desiccation process if the inoculation level is high, further increasing adhesion to surface... 56

Figure 32 #8 Mirror finish stainless steel was adequate for generating non-overlapping *Salmonella* Enteritidis PT30 on surface smooth enough not to trap bacteria in between the grain boundaries of the metal. This conclusion is important for the modeling of individual bacteria to detach off surface given an imposed force. .... 56

Figure 33 3-dimensional height retrace of individual *Salmonella* on surface, the Cypher AFM has the capability of reaching very small dimensions while measuring (~nm scale), showing individual roughness, and direct interaction with the bacteria in a physical state..... 57

## **CHAPTER 1. INTRODUCTION**

### **1.1 Background**

#### 1.1.1 Statistics for Foodborne Illnesses

According to Scallan et al. and the U.S. Center for Disease Control (CDC), approximately 48 million people in America get one form or another of foodborne illness a year, in which 128,000 are hospitalized, and 3,000 die (Scallan et al., 2011). From 1998 to 2014, there was an overall 29% decrease in foodborne bacterial and parasitic infections across the United States (Scallan et al., 2011). Despite this decreasing trendline, one major outbreak regarding a certain product can have immediate negative health impacts on the population and resounding economic impacts for the company and product associated with the incident for years afterward. By 2050 the global population is projected to reach 9 billion people (Hanjra & Qureshi, 2010). Based on current agricultural production, the world will face a serious food shortage. With increasing number of new technologies, distribution techniques, and more efficient conversion of land acreage to viable produce, the agricultural industry will be able to continue feeding the world. However, one local contamination event at any one of these steps could potentially lead to a nationwide foodborne illness outbreak with resounding implications.

#### 1.1.2 Low-Moisture Food Safety

Historically, food securities, demographics, and population demands have changed the dietary patterns. In the early 20<sup>th</sup> century, increased ability to process, distribute, and store foods has led to the development of many different dietary changes, and to the increased potential of facilitating the widespread distribution of foodborne pathogens to the public given an uncontrolled contamination event.

Processing methods for reducing foodborne illness have been developed throughout history, including pasteurization of milk to control milk-borne infections (Coldrey, 1943), and aseptic processing of canned foods to prevent botulism (Brown, 2000). As reporting procedures, processing standards, and fiscal/ethical accountability standards have improved, the number of reported foodborne pathogen outbreaks have decreased (CDC, 2016). However, foodborne outbreaks associated with low-moisture food products such as tree-nuts (Lambertini et al. 2012), wheat (Crumrine et al., 1971), and dried fruits (Beuchat & Mann, 2014) have been increasing in frequency. The reason behind of the increase is due to the negligence in that these products have traditionally been assumed as a low risk category due to the lack of ability for bacteria to proliferate in low-moisture environments in which water activity (defined as  $a_w = p/p_0$ , where  $p$  is the vapor pressure of water in product,  $p_0$  is the vapor pressure of pure water at the same temperature at equilibrium conditions) is one of the most critical factors limiting the growth state of bacteria. Therefore, water activity ( $a_w$ ) is controlled at product specific values all under 0.98 to prohibit bacteria from being active, which reverts the metabolic state of the bacteria to a dormant stage in that bacteria can survive for a prolonged period of time (Grocery Manufacturers Association (GMA), 2009). During this desiccated state, the bacteria physiologically respond attempting to withhold as much water as possible to remain a viable organism actively competing against direct moisture loss to environment. However, dormant bacterial cell can become active at higher water activities, which is one potential mechanism of foodborne illness via low-moisture food products.

Tree nuts are one of the important low-moisture commodities. California almonds were implicated in two outbreaks of salmonellosis in 2000 and 2003, which recalled ~6,000 metric tons of raw almonds in 2004 (Scallan et al. 2011). As a result of the outbreaks associated with

almonds (Danyluk et al., 2007), pistachios, peanuts, and sesame seeds (Isaacs et al., 2005) stricter food safety standards became necessary for low moisture products. Harvesting and processing of nuts such as almonds is executed in a low-moisture setting (Danyluk, et al., 2007), where there is still a lack of understanding of how *Salmonella* contamination occurs and along with potential prevention and mitigation techniques. Therefore, there is a growing need to investigate the root causes of low-moisture contamination of products and how the contaminated products spread through industrial settings (Kwakwa, 2006). The U.S. produces 80% of the world's almonds (Almond Board of California (ABC), 2016) and is the largest exporter, supplying an average of 970 million pounds to other countries (roughly ~3/4 of the world market). Hence, any food safety problems with almonds would serve to further weaken the U.S. position in the world market (Kwakwa, 2006; Harris et al., 2016). To mitigate future outbreaks, understanding of bacterial contamination and implementation of multiple strategies of intervention is needed for sectors such as tree nuts in low-moisture environments. In addition, the Food Safety Modernization Act (FSMA) introduces a regulatory process of food manufacturers utilizing cGMP (Current Good Manufacturing Practice) and risk-based preventative controls to mitigate the risk associated with the bacterial transfer (Food and Drug Administration (FDA), 2010). However, there is a significant lack of understanding about cross contamination of pathogens in dry products. To meet this challenge, a more fundamental approach is necessary to elucidate the mechanisms of *Salmonella* attachment/transfer to the surface of low moisture foods, contact surfaces, and the processing environments.

### 1.1.3 Why Cross-Contamination Matters

Introduction of microbial pathogens into a food processing environment can occur at any stage: pre/post-harvest to post-processing handling (Danyluk, et al., 2007). In the case of the

almond salmonellosis outbreaks in 2000 and 2003, *Salmonella* likely entered the facility on the raw product (Lambertini et al., 2012), since almonds are collected from the ground. Significant meteorological events, such as heavy rainfall, increases the risk of *Salmonella* contaminating the almonds still on the ground. Once the pathogen is absorbed into the drupe, the potential for further spread of the pathogen is high throughout the rest of the low moisture process due to the cross-contamination of detached bacteria from the contaminated almond.



Figure 1 Almond harvesting process that sweeps dried almonds on the ground (courtesy of [www.almond.com](http://www.almond.com))

Other sources of contamination in low moisture environments could occur during or after processing. All operations have multiple critical points that processing facilities must appropriately implement their risk based preventative control plans to, because the hazards of contamination will be inherent to any system processing products obtained from nature. FDA regulations state that tree-nuts such as almonds must be treated to achieve a validated 4-log reduction for *Salmonella* as of 2007 (7 CFR Part 981, 2007) (Food and Drug Administration, 2010). In order to further assess the hazard and reduce the risk of outbreaks associated with low moisture foods, a comprehensive assessment of all safety implementation techniques, such as kill step verification and validation of pathogens, must be performed. In addition to the assessment,

understanding the initial contamination event and further cross-contamination events afterward from product-to-environment, and vice versa will provide critical information and knowledge to ensure overall low-moisture food safety and will further assist the development of prevention and cleaning techniques, implementing strategies that efficiently prevent hazards and eventually increase public safety.

## **1.2 Pertinent Literature Review**

### **1.2.1 Previous Approach**

Conventional approaches of investigating contamination of low-moisture products such as almonds utilize experimental results and approximate mathematical models based on empirical results and data curve fits (Sheen & Hwang, 2010). A probability-of-transfer model is often used, where the “transfer rate” is just the fraction (probability) of the initial cells transferred for a given contact event however, only studied in high moisture environments (Pérez-Rodríguez et al., 2007). The challenge in these cases is that transfer rates vary greatly due to multiple factors such as environmental conditions and type of bacteria (Pérez-Rodríguez, et al., 2007). Although empirical approaches can provide directly relevant results for the specific cases, utilizing empirical results in a laboratory model have a limited scalability on real life applications, such as industrial scale validation. Due to the cost and impractical nature of contaminating low-moisture products with pathogens at an industrial scale, alternative modeling approaches are needed for practicality.

### **1.2.2 New Approach**

As opposed to the empirical approach (or black box method) to study cross-contamination phenomena, new approaches (or white box method) for understanding experimental results is to expand from the theoretical first principle interactions of what is happening in micrometer scale.

First principle models are defined as models derived directly from the fundamental laws of nature; for example, Newtonian physics and Coulomb interactions (Banga, Balsa-Canto, Moles, & Alonso, 2003). The advantages of first principle models are the ability to minimize any uncertainty of scaling up the experimental results from the laboratory to industrial environments.

In order to take the first principle based approach, a better understanding of the phenomena is needed to figure out the fundamental mechanisms. Bacteria such as *Salmonella* that attached to surfaces with flagella are utilizing the Coulomb interaction between the flagella and the surface to remain attached in an aqueous environment. However, since in low-moisture environments the flagella deteriorate and become irrelevant, only cell surface forces contribute to their attachment to any surface. Particle by particle contact mechanics as described by the Hertzian contact models (Johnson, Kendall, & Roberts, 1971) could properly assess the propagation of colloidal objects, with many additions to the basic Hertzian model accounting for factors such as geometry, deformation, and adhesion properties. Characterizing both the small and medium scale interactions into one system by first principle reactions can be utilized to obtain statistically sound large-scale results. Implementing a model based on Coulomb forces keeping bacteria attached to a larger particle such as an almond and the Hertzian contact force between larger particles to calculate the collision contact area of bacteria transferred can provide a better understanding of cross-contamination in low moisture environments. Therefore, the first principle based approach has distinct advantages of being able to apply the techniques across multiple topics and disciplines. For instance, Benoit discussed that understanding the same mechanics of bacterial adhesion and detachment due to external forces can be applied to bacteria transfer risk associated with deli slicing machines, before continuing to develop an empirical transfer model (Benoit, 2013). In addition to being robust across different topics, first principle

based approaches to creating a laboratory scale model is directly relevant to the industrial scale with minimal approximations or assumptions. Thus, the accurate and robust model for cross contamination phenomena will enhance risk assessment tool for industrial settings.

### **1.3 Objectives**

Research presented in this thesis was conducted with the overall goal of food safety in low-moisture food products, by increasing the knowledge of the cross-contamination phenomena at the fundamental level. Therefore, the specific objectives were:

1. To develop an exploratory first principle based discrete element model for adhesion of bacteria to food contact surfaces in low moisture environments.
2. To measure adhesion forces of individual cells directly/indirectly and the related physical parameters using actual *Salmonella*.
3. To validate the discrete element model using the measured micro-scale adhesion parameters by simulating a macro-scale experiment.

## CHAPTER 2. THEORIES

### 2.1 Adhesion Theories

#### 2.1.1 Background Knowledge

Given the presence of water and nutrients, bacteria can proliferate and produce a biofilm. In a biofilm, microorganisms are in a healthy environment allowing cell division, extracellular matrix (ECM) production, and fostering an environment for more microorganisms to be released from the biofilm as well (Araújo et al., 2009). However, before biofilm formation, bacterial adhesion must first occur, which can happen in an aqueous solution, or in a desiccated environment where water is later introduced. A microorganism's tendency to adhere to surfaces is a survival mechanism for the initial advancement of developing a biofilm. Also, it is widely discussed if pathogenic microorganism has stronger adhesion mechanics to other similar organisms or not (Haiko & Westerlund-Wikström, 2013; Kalmokoff et al., 2001). Given the initial dislodging and transfer of a bacterial cell from one surface to another, there are two stages of adhesion before biofilm production: reversible mechanics, and irreversible mechanics. The reversible stage occurs when the amount of work required to approach the surface is equal to the amount of work required to retract from the surface. Only long-range forces such as Van der Waals and electrostatic interactions account for the reversible interaction range shown in Figure 2. Irreversible region begins when the distance from the microorganism body to the surface is  $<1.5$  nm where ionic links, hydrophobic forces, and electron donation-accepting pairs occur (Araújo et al., 2009). When discussing the initial adhesion of bacteria to a surface, only the reversible kinetics are of concern.

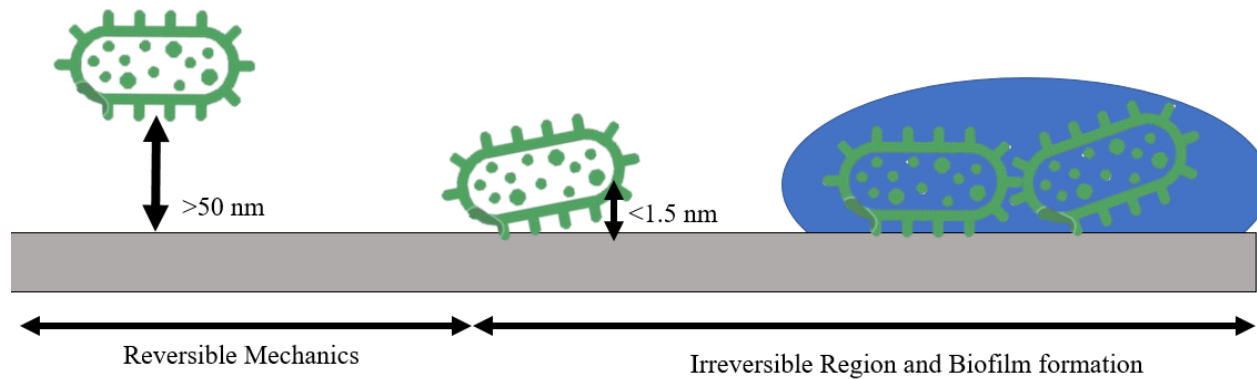


Figure 2 Interaction of a bacterial cell with a solid surface (Araújo, et al., 2009).

#### 2.1.1.1 Parameters of Bacterial Adhesion

Bacterial adhesion is a function of many different parameters: cell surface properties, lipopolysaccharides (LPS), growth conditions, environmental factors, and the species of bacteria (Hori & Matsumoto, 2010). In addition, the surfaces to which the bacteria adhere have varying properties of roughness and surface interaction forces. In general, these physical and chemical characteristics can be accounted for in mathematical terms, accounting for surface energy and environment factors. One mathematical explanation of the adhesion force interactions between colloids is the DLVO (Derjaguin and Landau, Verwey and Overbeek) theory (Hermansson, 1999). The DLVO theory has been commonly applied to the adhesion of microorganisms (Hori & Matsumoto, 2010; Rijnaarts et al., 1995). It combines the effect of Van der Waals forces and double layer forces of colloids and surfaces to obtain effective colloid dispersion. In the microbiological literature, DLVO equations are commonly applied to describe the thermodynamic stability of microorganisms in different solutions.

### 2.1.1.2 DLVO Equations

For a sphere approaching a surface, the interaction energy by the van der Waals force is:

$$W(D) = -\frac{2\pi C\rho_1\rho_2}{12} \int_{z=0}^{z=2R} \frac{(2R-z)zdz}{(D+z)^3} \approx -\frac{\pi^2 C\rho_1\rho_2 R}{6D}$$

Equation 1

Where  $D$  is the distance from the surface,  $C\rho_1\rho_2$  is the effective constant interaction energy multiplied by the sphere and surface number densities,  $R$  is the radius of the particle, and  $z$  is the coordinate within the particle of  $R$  radius. For convenience, the Hamaker constant is denoted as  $A = \pi^2 C\rho_1\rho_2$  reducing Equation 1 to:

$$W(D) = -\frac{AR}{6D}$$

Equation 2

The double layer force is specific to particles and surfaces submerged in liquids where a charged dissociation may occur depending on the pH and electrolytes in the solution. The repulsive energy of two planar surfaces (or a colloid and surface from far away) is shown as

$$W(D) = -\frac{64k_B T\rho_\infty\gamma^2}{\kappa} e^{-\kappa D}$$

Equation 3

Where  $k_B T$  is the Boltzmann temperature,  $\rho_\infty$  is the ion density in the solution,  $\gamma$  is the surface energy of the colloid, and  $\kappa$  is the Debye length proportional to the electric double layer for the solution. Figure 3 shows how the double-layer repulsion force and van der Waals force compete forming an energy barrier to achieve an attractive relationship between two particles distance  $D$  away from each other.

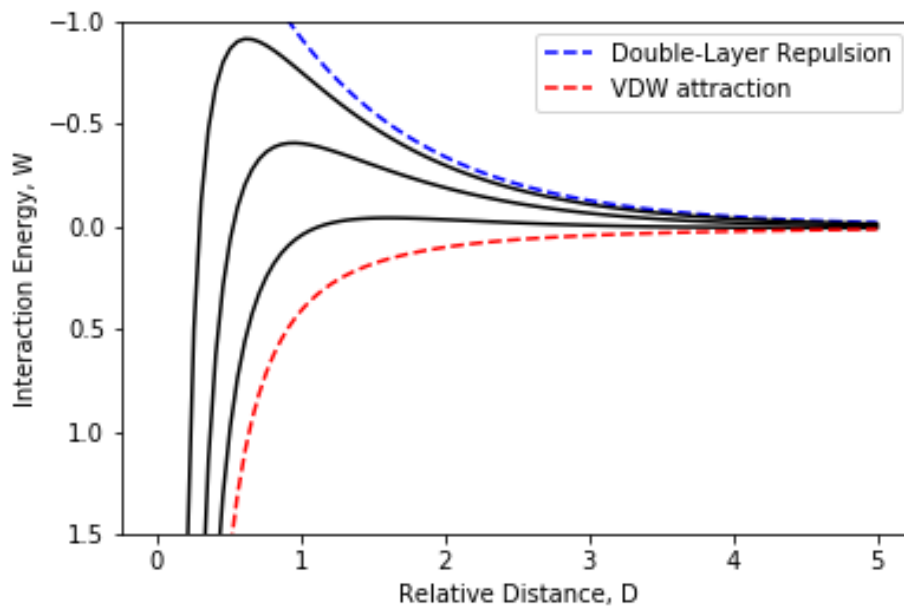


Figure 3 DLVO Interaction energy of colloids interacting in an aqueous solution, showing the Double-Layer Repulsion (blue dotted line), and the van der Waals attraction (red dotted line) limits, and the competition between the two forces (black lines), in dimensionless units (Israelachvili, 2011).

The combination of the Van der Waals and double layer interaction energy determines the total particle interaction with a surface or another particle (in this case microorganisms). Note that Van der Waals is an attractive force and the double layer interaction energy is a repulsive force.

$$W(D)_{tot} = W(D)_{vdW} + W(D)_{edl}$$

Equation 4

Due to the inconvenience of measuring the instantaneous energy of a microorganism with respect to a surface, the thermodynamic law of the minimum Gibb's free energy for a system at equilibrium is applied to the DLVO concept. Lower Gibb's free energy suggests it is more energetically favorable adherence to a surface than another environment.

$$\Delta G_{adh} = \Delta G_{vdW} + \Delta G_{edl} + \Delta G_{additional}$$

Equation 5

Taking the thermodynamic limit allows for the ability to observe microbial surface thermodynamics (Araújo et al., 2009).

$$(1 + \cos \theta)\gamma_L = 2 \left( \sqrt{\gamma_S^{LW}\gamma_L^{LW}} + \sqrt{\gamma_S^+\gamma_L^-} + \sqrt{\gamma_S^-\gamma_L^+} \right)$$

Equation 6

Where  $\gamma_L$  is the surface tension of the liquid,  $\gamma_{S,L}^{LW}$  is the van der Waals component of the surface tension for both the solid (microbe) and liquid respectively, and  $\gamma_{S,L}^{+,-}$  is the electron acceptor/donor parameter for the solid and liquid respectively as well. Multiple surface tension measurements obtained in known liquids can be used to assess microbial surface thermodynamics. Conveniently, the contact angle of a liquid on a surface can be physically observed by placing a droplet of the microbe and solution mixture on a surface of known surface energy.

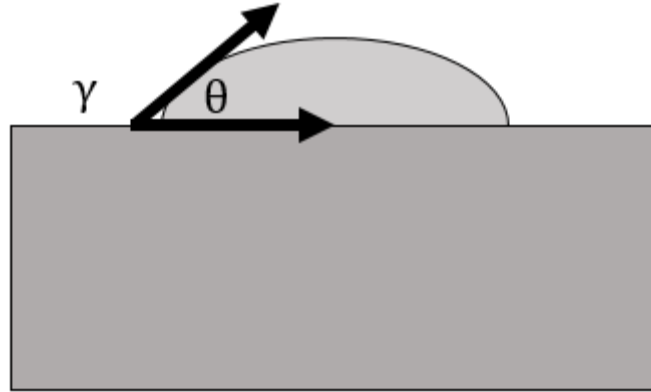


Figure 4 Contact angle between a surface and the liquid, can be used to calculate the surface energy level ( $\gamma$ ) of the microbes in the liquid solution (Israelachvili, 2011).

The DLVO theory properly constructs a mathematical description of bacterial adhesion based upon many factors (Hermansson, 1999; Araújo et al., 2009). However, these equations only apply for microorganisms in aqueous solutions and only provides a solution at thermodynamic equilibrium, which does not account for many considerations such as surface deformation or other forces acting on the system. Also, to obtain the surface energy parameter for every bacteria strain, general model must be experimentally calibrated at multiple contact angles, which is very time consuming with large uncertainty and inability to expand to other environments. Consequently, more robust models for bacterial adhesion that can be applied to low moisture environments is needed.

### 2.1.2 JKR Cohesion for Particulates and Granular Physics

Two elastic particles with no adhesion interaction ( $F_{ad} = 0$ ), will exhibit free kinematics to them. Upon collision, their elasticity, based upon the Young's modulus, will dictate the extent of deformation, energy loss, and the respective physical consequences. The Hertzian contact equation states that the contact radius  $a_0$  of a collision event is given by:

$$a_0^3 = \frac{RP_0}{E^*}$$

Equation 7

$$R = \frac{R_1 R_2}{(R_1 + R_2)}$$

Equation 8

$$E^* = \frac{4\pi}{3}(E^1 + E^2)$$

Equation 9

Where Equation 8 is the effective radius of both particles with radii ( $R_1$ ,  $R_2$ ),  $P_0$  from Equation 7 is the load, and  $E^*$  from Equation 9 is the effective Young's modulus of individual moduli  $E^1$ ,  $E^2$  (Johnson, et al., 1971). If adhesion between two surfaces is present the Johnson, Kendall, & Roberts (JKR) Theory states that the contact area,  $a_{jkr}$ , will alter as a function of the work of adhesion.

$$a_{jkr}^3 = \frac{R}{E^*} \left[ \sqrt{\frac{3}{2}\pi RW} \pm \sqrt{F + \frac{3}{2}\pi RW} \right]^2$$

Equation 10

With  $W$  being the work of adhesion, and  $F$  is the force applied to the particle, if the contact area is proportional to the work of adhesion, applying a constant removal force to a particle from a surface will result in a detachment of the particle at the critical adhesion force  $F_{ad}$  (Johnson, et al., 1971).

$$F_{ad} = -\frac{3}{2}\pi RW = -3\pi R\gamma$$

Equation 11

Where  $2\gamma = W$ , or the work of adhesion is twice the surface energy density of the particle. Figure 5 shows the deformation of an elastic particle on a surface at equilibrium. Given a constant pull off force applied the particle remains in contact with the surface, until the pull off force is equal to  $F_{ad}$ .

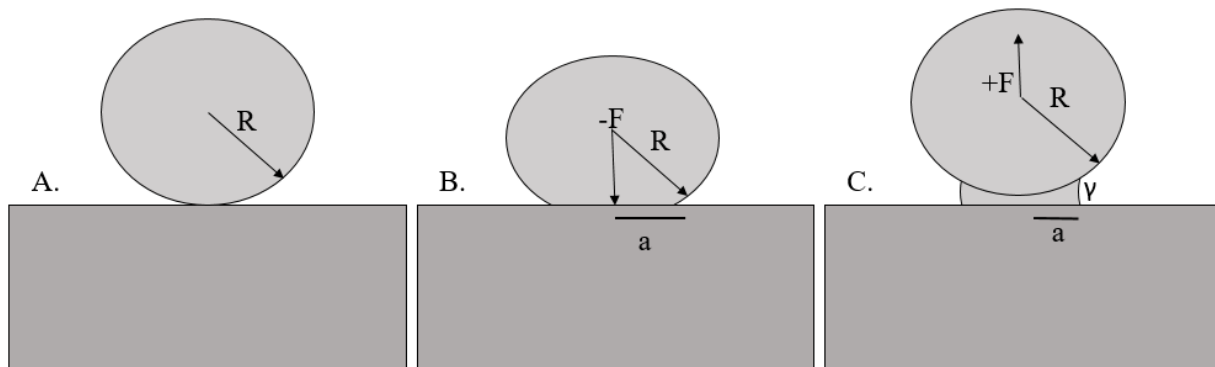


Figure 5 Comparison of JKR theory for: A a rigid sphere, B. a deformed sphere from a downward force, and C. a positive force and resistance to detachment by the surface energy, consistent with the JKR theory (Israelachvili, 2011).

Also, the work of adhesion  $W$  is equal to  $2\gamma$  twice the surface energy in the respective boundary (Solid-Liquid, Solid-Vapor), meaning that measurements of surface energy can equally apply to the JKR theory, in addition to the DLVO theory.

The JKR theory has several advantages in that it describes adhesion in kinematical terms, is independent of the environment, and can describe reversible and irreversible adhesion characteristics of colloids. There is a distinct lack of literature applying the JKR Theory to

microbiological organisms, mainly because most microbiological measurements of concern are in aqueous environments. With the increase of concern of pathogens in low-moisture environments, it will be advantageous to apply the JKR theory to obtain more meaningful insight on cross-contamination and bacterial propagation in other than aqueous industrial environments.

### 2.1.3 Adhesion Measurement Techniques

#### 2.1.3.1 Atomic Force Microscopy

The actual adhesion force of bacteria can be measured using Atomic Force Microscopy (AFM) (Razatos, Ong, Sharma, & Georgiou, 1998). AFM is operated by taking a very precise cantilever with a  $<1$  nm thick tip and dragging the tip across the surface of interest. By determining the deflection of the AFM needle, a 3-dimensional reconstruction of the surface can be obtained at the  $<1$  nm resolution. In addition, AFM tip-less cantilevers can be used to perform larger scale ( $\sim 1$   $\mu\text{m}$ ) measurements of adhesion force by fixing bacteria to the cantilever and approaching and retracting the device at many different locations on a surface (Bowen et al., 2001; Huanget al., 2015). The single-cell adhesion force obtained by AFM can have multiplicative impacts on other fields of research. Razatos et al.,(1998), Bowen et al.(2001), and Huang et al.(2015) have well established protocols to obtain adhesion force data, however, their work has been limited to aqueous environments.

#### 2.1.3.2 Centrifuge Technique

In addition to the micro-canonical scale of the first principle-based adhesion measurements using AFM, the actual adhesion force must also agree with the macro-scale results as well. Theoretically, lack of agreement of individual measurements with large-scale results may lead to an inconsistent implementation of the model.

A novel approach to grand adhesion force measurements can be performed by implementing a centrifuge, common to most microbiology labs, with particles of interest adhered to inner surface of interest inside a centrifuge tube. Ensuring sufficient space between the bottom of the tube and the particles at the surface, operating the centrifuge at multiple RPMs and measuring the difference in particles from the beginning to the different centrifugal force amounts applied would yield a statistical distribution of adhesion forces.

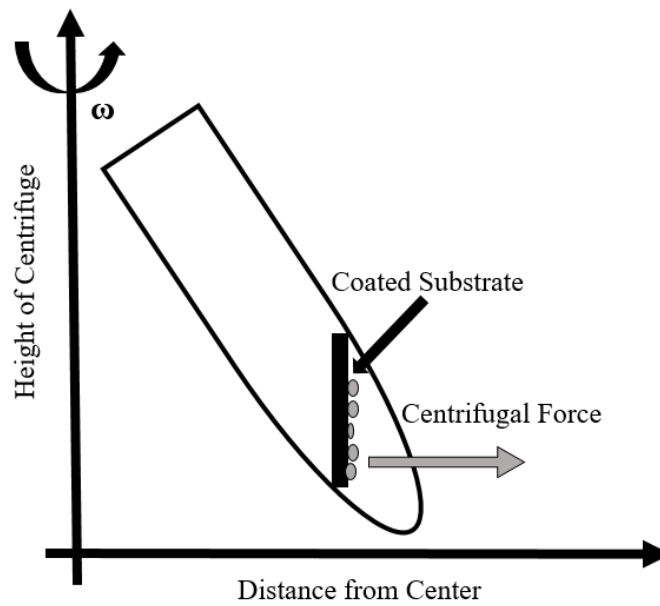


Figure 6 Determination of adhesion force, where a sample is held in the centrifuge vial and is detached in the normal direction of the force as the sample rotates (You & Wan, 2014).

Many other disciplines concerned with colloids and adhesion of particles to surfaces have successfully utilized this technique from Aerospace engineering (You & Wan, 2014) to granular food particulate adhesion (Ermiset al., 2011). All models of centrifugal force detachment account for the JKR theory of particle adhesion. Comparing the centrifugal force (Equation 12) to the JKR Adhesion Force (Equation 13), the statistical median adhesion force and confidence intervals can be calculated by applying Monte Carlo techniques to the process.

$$F_{cen} = m\omega^2 d$$

Equation 12

$$F_{ad} = -\frac{3}{2}\pi RW$$

Equation 13

Once the experimental micro and macro measurements can be confirmed and validated, implementation of adhesion data to model systems can be used to further elucidate the bacterial cross-contamination phenomena and adhesion mechanics.

## 2.2 DEM Modeling

In order to implement first principle approaches, a system that can most accurately describe the physical phenomena of bacterial adhesion must be in place. A theoretical mathematical model of bacterial transfer by collisions can provide insight and be applied to a computational simulation. The Discrete Element Method (DEM) is a computational simulation technique used to compute individual particle movements and interactions with no approximations between time steps. DEM holds the distinct advantage of being able to track individual movements of multiple particles of a bulk material, by applying the first principle interactions between all particles in large scale environments. LIGGGHTS (LAMMPS Improved for General Granular and Granular Heat Transfer Simulations) is a DEM toolkit specializing in the modeling of bulk material transport on the order of  $10^{-5}$  to 100 m in scale (Kloss, Goniva, Hager, Amberger, & Pirker, 2012). LIGGGHTS has been implemented in many industrial applications such as solids (Kwapinska et al., 2006), granular flow (Nguyen et al., 2012) and fluidized beds (Goniva et al., 2012).

However, bacterial transfer simulations have not been performed utilizing DEM. Based upon molecular dynamic simulation techniques, LIGGGHTS is designed to correctly calculate granular physical interactions with molecular forces. Bacterial cross-contamination simulations can be accomplished within LIGGGHTS utilizing the independently theoretical model of cross-contamination and the first principle interactions to provide insights into the microbial interactions in a scaled-up environment otherwise overlooked by conventional methods of experimentation.

LIGGGHTS has the capability of implementing the JKR model for particles and can approximate complex geometries, using multi-sphere rigid bodies (Kloss et al., 2012). This concept can then be applied to simulate microbes. With the measured experimental properties, a DEM model can be simulated to reveal previously unobservable mechanics and phenomena in the process. Due to the complexity of the simulations, parallel computing resources such as Michigan State University's High-Performance Computing Center (HPCC) can be utilized to perform the simulation efficiently and economically in terms of computing time and resources.

## CHAPTER 3. METHODS AND PROCEDURES

### 3.1 Overall Approach

To achieve the objectives of the thesis, multiple experiments were performed to obtain adhesion force data, such as bacterial size, shape, and mass which are essential to properly model the first principle-based adhesion phenomenon. Size, mass, adhesion force of single cell were measured by using microscopy technologies, such as SEM (Scanning Electron Microscopy) or AFM (Atomic Force Microscopy), and also statistical quantification method using the centrifugal method. Given the focus of this work on low-moisture environments, *Salmonella* Enteritidis PT30 was chosen as the pathogen of concern, with stainless steel 304 as the food contact surface. *Salmonella* Enteritidis PT30 culture was obtained from Dr. Linda Harris (University of California Davis). The strain was preserved at -80 °C in tryptic soy broth (TSB) (Difco, 2009) containing 20% glycerol. Before each experiment a loop from the original frozen culture was subjected to a minimum of two consecutive 24h/37 °C transfers in TSB. The objective of the experimental approach was to perform both microscale and macroscale measurements in junction with DEM modeling techniques to validate model results (Figure 7). In addition, direct application of microscale measurements to explain macroscale phenomena can be assessed between the two results directly.

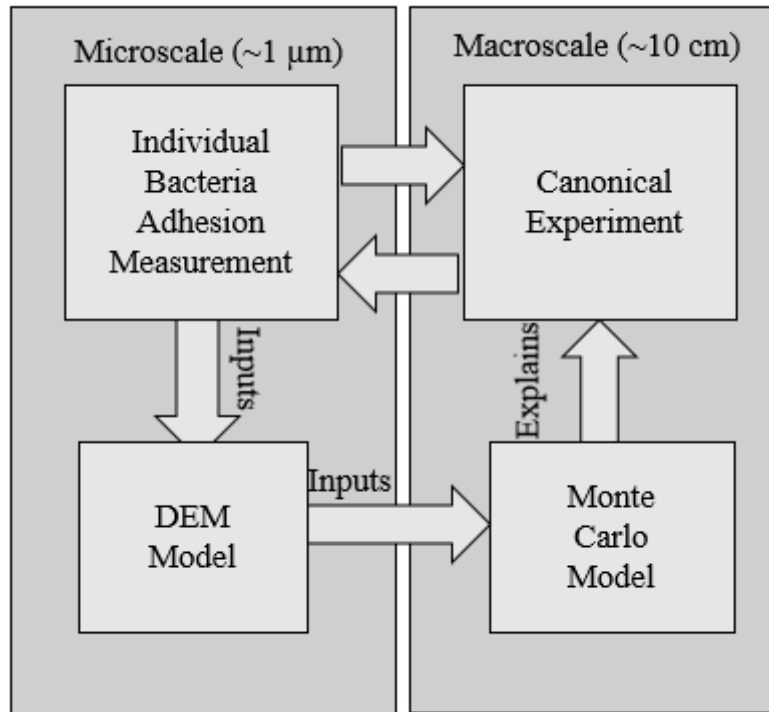


Figure 7 Overall approach for acquisition of individual bacterial measurements, application of results to a first principle based DEM model, and explanation of the large scale canonical experiments using Monte Carlo modeling

### 3.2 Mass of Bacteria

Prior literature review in regard of individual bacterium mass measurements has shown a lack of reported uncertainty, with conflicting results between sources, and few variations of environments such as low-moisture conditions. For bacteria in a desiccated state, there is a significant decrease of water to the system. However, over 60% of the total water from a bacterial pellet is intercellular water (Bratbak & Dundas, 1984) even at a desiccated state. The accuracy of reported masses of individual bacteria of similar shape and size are only within an order of magnitude of approximately one picogram (Bratbak & Dundas, 1984). Therefore, a simple experiment was performed to get a distribution of mass measurements of individual *Salmonella* cells in reference to the literature. Cultures obtained as mentioned in Section 3.1

were incubated in 6 individual 10 mL vials of TSB. Cultures were transferred and centrifuged at 5,000 RPM (relative centrifugal force, RCF= 2988 x g) (Sorvall RC6+ SS-34 holder) for 15 min. Thereafter the supernatant was discarded and bacteria were resuspended in 10 mL of 0.1M phosphate buffer solution (PBS) then centrifuged again. After the PBS was removed, the six bacterial pellets were each suspended with 1 mL of PBS and placed in an individual aluminum weighing dishes and weighed with the analytical balance ( $\pm 0.0001$  g). Three negative controls containing just 1 mL of PBS per experiment were also included. Enumeration of samples was performed by 1:10 serial dilutions in buffered peptone water (BPW) solution, plated 100  $\mu$ L of each dilution on modified Tryptic Soy Agar (mTSA) and incubated at  $37^\circ \pm 1^\circ$  C for 48 h to obtain a final population reported as Colony Forming Units per mL ((CFU)/mL). For modeling purposes, all additional Extracellular Matrix (ECM) and nonviable cells remaining after the washing of the cells was agglomerated in the total CFU mass consideration. The samples in measuring dishes were desiccated over 24 h in a hermetically sealed chamber layered with desiccant, and final mass was recorded. Experiments were performed in triplicate to ensure reproducibility, taking the ratio of final CFU/mL concentration performed and the final dry mass of each weighing dish to obtain the mass per CFU (Equation 14). This experiment was performed as a proof of concept to obtain empirical mass results by macro-scale techniques, due to lack of literature. Although the cell state will not be entirely desiccated, the mass of the cell after a 24 h desiccation period was used as a representative mass indicative to an low-moisture ambient processing environment.

$$\frac{\text{Mass of CFU}}{\text{mass of sample (g)}} \approx \frac{\text{Number} \frac{\text{CFU}}{\text{mL}}}{\text{mass (g)/mL of inoculum desiccated}}$$

Equation 14

### 3.3 Size and Shape of Bacteria

Scanning Electron Microscopy (SEM) was used to determine the size and shape of *Salmonella* Enteritidis PT30. Inoculum was prepared from frozen culture and resuspended in 10 mL of TSBYE then transferred to another vial of 10 mL TSBYE after a 24 h period of incubation. After a second transfer, the inoculum was pelleted at 5,000 RPM (RCF=2988 x g). The supernatant was removed and the pellet was resuspended in 0.1 M Phosphate Buffer Solution (PBS) to be used as the initial solution for the preparation of scanning electron microscopy (SEM) samples.

As the attachment surface, food grade 304 stainless steel coupons (22 mm x 22 mm #8 mirror finish) were pretreated in acetone for 15 min to ensure a clean surface, and washed with distilled water afterward. Samples were then placed in 9 mL of PBS containing one mL *Salmonella* inoculum solution in a 50 mL beaker to ensure the entire top surface of the sample was submerged. The stainless steel coupon was then gently agitated with a bench top linear shaker in rocking motion at 60 RPM at room temperature (~21° C) for 2 hours. The sample was gently agitated to ensure strong attachment and even distribution of bacteria across the surface. The inoculated stainless steel coupons were then removed and placed in an environmental conditioning chamber at 45% RH for 24 hours to desiccate the bacteria.

Because of the pathogenic nature of *Salmonella*, the inoculated stainless-steel samples were irradiated for 10 minutes at an approximate dose of 50 kGy using a prototype X-ray irradiator (Rainbow™ II, Rayfresh Foods Inc, Ann Arbor, MI) to ensure inactivation of *Salmonella* for SEM before leaving the Biological Safety Level 2 laboratory.

Preparation of samples for SEM started by placing the stainless steel coupons in 2.5% glutaraldehyde for 2 hours to fix the bacteria. After fixation, the stainless steel coupon was rinsed in PBS for 15 minutes to remove any loosely attached cells and debris leaving the strongly attached cells. Serial dehydration of cells on the coupon was accomplished using ethanol solutions of 30%, 50%, 70%, 90%, and 100% for 10 minutes each, followed by 100% ethanol solution for 1 hour. After dehydration, the sample was dried in a CO<sub>2</sub> critical point dryer for 15 minutes, and then sputter coated with a 5.5 nm layer of iridium for SEM imaging.

After SEM pictures of bacteria evenly distributed on a stainless-steel surface were obtained, computer image analysis of the shape and size of individual bacterial cells was done using ImageJ (Schneider et al., 2012), an image processing and analysis program for particle measurement and analysis from images. The image files were loaded into the program with regions of interest (ROI) then selected. Because *Salmonella* is known to be a rod-shaped bacterium which can be approximated as an ellipsoid for measurement purposes, the major and minor axis of the ellipsoid shape and the circularity of a cell (Equation 15) were determined individually by methods described in Schneider et al. and agglomerated with multiple measurements for statistical analysis based on Gaussian fit distributions using normality fit by Shapiro-Wilk Normality test (Shapiro S. S. & Wilk, M. B., 1965).

$$Circularity = 4\pi \frac{Area}{Perimeter^2}$$

Equation 15

### 3.4 Direct Measurement for Bacteria and Surface Characterization Using AFM

To obtain single-cell force measurements and individual cell AFM images, *Salmonella* Enteritidis PT30 cultures were prepared on two different types of Food Grade 304 stainless steel #8 mirror finish and #4 brushed. The #8 mirror finish is a premium surface finish seldomly used for food manufacturing equipment, however the #4 brushed finish is widely used food processing equipment (United States Department of Agriculture (USDA), 2001). Different finishes of stainless steel were used to observe if surface roughness influences bacterial adhesion. AFM was later used to determine the root mean square roughness (RMS) of each surface finish (Equation 16) where  $Z_i$  is the  $i$ -th height measurement of the surface, and  $N$  is the total number of height measurements. The method of sample preparation for AFM imaging purposes were prepared as described in Section 3.3.

$$\text{Root Mean Square Roughness} = \sqrt{\frac{1}{N} \left[ \sum_{i=1}^N Z_i^2 \right]}$$

Equation 16

A Cypher AFM (Asylum Research, Santa Barbara, CA) machine was used to obtain the atomic force measurements and images. Using the inoculated stainless steel samples as prepared for SEM imaging, a 300 kHz Silicon Nitride (SiN) fine point tip was used to obtain topographic images of the surface and bacteria in the AFM tapping mode with scanning areas from  $2 \mu\text{m}^2$  to  $200 \mu\text{m}^2$ .

To obtain consistent adhesion measurement data, a PBS suspension of SEPT30 was spot inoculated directly onto the stainless the surface (Figure 8). Using a gold coated Pyrex-Nitride

Probe (PNP) tip-less cantilever (Asylum Research, Santa Barbara, CA) (Figure 8), a mapping of the adhesion force could be performed to a  $20 \mu\text{m}^2$  area, to obtain the force interaction between the cantilever-bacterium and cantilever-surface.

In order to obtain bacterium-surface and bacterium-bacterium force measurements, cells were adhered to the cantilever. Cyanoacrylate (i.e. adhesive) was applied to the end of the tip-less cantilever by first touching the cantilever to a cyanoacrylate droplet on an uninoculated area of the stainless surface, followed by moving the wetted cantilever to an inoculated area on to fix the cells onto the cantilever. After the cyanoacrylate dried for 10 minutes on the inoculated area, the cantilever, with *Salmonella* adhered to the surface of the cantilever, performed the same force mapping to an uninoculated  $20 \mu\text{m}^2$  area for bacterium-surface interactions, and to an inoculated area for bacterium-bacterium interactions. The bacterium-surface and bacterium-bacterium force interactions are the direct adhesion force measurements concerning the reversible force interactions that can be directly applied to the JKR theory. By observing the deflection of the tip-less cantilever when applied to an individual bacterium, the Young's Modulus of the bacteria can be estimated by Cypher AFM's internal routine, fitting the  $E_1$  from Eq. 9 using a nonlinear wOLS routine.

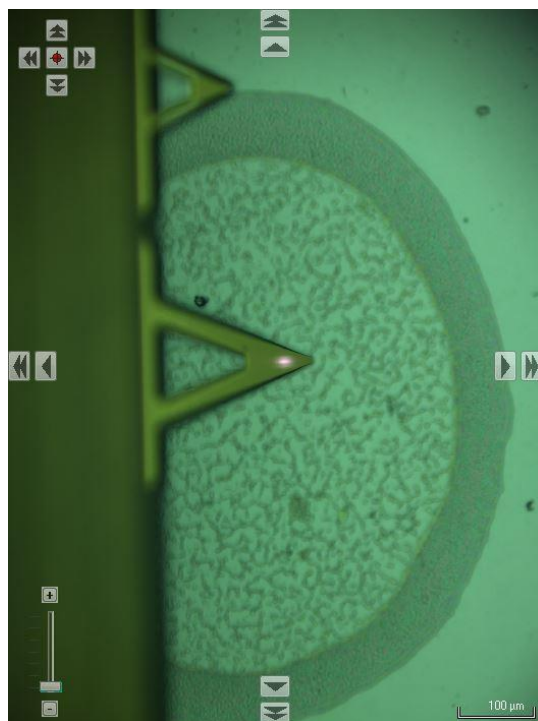


Figure 8 Optical microscope image of Au coated tip-less PNP AFM cantilever and a dense population of bacteria on the surface. The tip-less cantilever was used to measure adhesion force on bacteria.

### 3.5 Statistical Quantification Using Centrifuge

#### 3.5.1 Inoculation and Sample Preparation

Stainless steel coupons were inoculated as described in Section 3.3 for SEM imaging. An apparatus to hold the stainless-steel coupons (Figure 9) inside the centrifuge sample holder (Sorvall RC-6+ SS-34) was fabricated using high density polyethylene (HDPE), ensuring that the sample is always in the normal direction of the centrifugal force, and is sufficiently separated (10 mm) from the bottom of the centrifuge tube (Figure 10). Stainless steel coupons were then secured inside the apparatus and placed into the centrifuge sample holder. After that, the samples were centrifuged without any liquid at varying speeds from 10.8 to 38,724  $\times g$  to find the critical range for bacterial removal in dry condition. After the experiment, the stainless steel coupons

were collected and washed with 5 mL of PBS for 2 min then serially diluted for enumeration of *Salmonella*. The data points were used to quantify bacterial adhesion and analyzed by a student's t-test.



Figure 9 Stainless steel 304 #4 brushed (left) #8 mirror finish (right) coupons used in the centrifuge experiment for measuring critical attachment force of *Salmonella* Enteritidis PT30 in a low-moisture environment.



Figure 10 Centrifuge sample holder (left) inserted in centrifuge tube (right) used for a centrifuge block (SS-34). Fabricated in the Department of Biosystems and Agricultural Engineering Shop, Michigan State University (East Lansing, MI).

### 3.6 First Principle Based DEM Modeling

After obtaining parameters for individual cell, such as dimensions, the force of adhesion, Young's Modulus, and the JKR contact area, a first principle based DEM model was developed. To simulate a real-life incident where bacteria are deposited on a surface at a certain concentration, model bacteria were created as multi-spherical objects based on the average dimension sizes found by the SEM (Section 3.3) and physical properties measured by the AFM (Section 3.4). The model bacteria shape was created by methods described in Amberger et al. with a particle count of  $n=50$ , and ellipsoid dimensions obtained from SEM images obtained from Section 3.3 (Amberger et al., 2012), the method describes approximating larger objects by the joining of a fixed number of smaller spheres as a rigid body, filling in the volume of the object closely as possible. These model bacteria were then deposited onto a smooth surface, and a linearly increasing force was applied to the time steps of the simulation. All model bacteria were given the same properties; the only random variance was initial deposition of the particles on the surface. LIGGGHTS was used to internally calculate the adhesion mechanics for all kinematics by the simplified JKR theory  $F_{ad} = kA$ , where  $A$  is the contact area, and  $k$  is the surface energy density ( $J/m^3$ ). The code implementing the DEM model simulation is provided in Appendix C as LIGGGHTS DEM CODE.

### 3.7 Monte Carlo Modeling

To implement the JKR theory of adhesion to individual particles on a surface, a Monte Carlo simulation was used to model the detachment of bacteria as centrifugal force increases in a pseudo-random environment. Monte Carlo simulation and parameter estimation was utilized to directly relate the individual measurements in Sec. 3.2 and Sec. 3.3 to the empirical results from Sec. 3.5. Referring back to Figure 8, providing Monte Carlo model results to explain the

empirical results would help determine adhesion parameters from laboratory scale experiments without further individual level measurements, or understanding of the parameter distributions.

The Pseudocode is as follows (The actual code is in Appendix C under MONTE CARLO SIMULATION PYTHON CODE):

1. Initialize number of bacteria with weight and size distribution and initial surface energy density value
2. For increasing centrifugal force:
  - a. Calculate if bacteria will detach by Metropolis-Hastings algorithm (max
    - i.  $F_{ad} = kA$
    - ii.  $F_{cent} = mr\omega^2$
    - iii. if  $F_{cent} > F_{ad}$  detach, else remain
  - b. Tally total number of bacteria still attached
  - c. Iterate for all centrifugal forces
3. Compare simulation to experiment, and optimize the surface energy density value.

The distribution of bacteria dimensions and mass determined from Section 3.2 and Section 3.3 were implemented in the Monte Carlo algorithm to form a distribution of simulated bacteria. The methods for the Monte Carlo Metropolis-Hastings algorithm are detailed in Armingier et al., where the surface energy density,  $k$ , from equation  $F_{ad} = kA$  was the parameter estimated by Bayesian likelihood (Armingier et al., 1998). The objective of the Monte Carlo modeling is to obtain the adhesion information given the empirical centrifuge test and individual bacteria information using large-scale results to obtain micro-scale fundamental information.

## CHAPTER 4. RESULTS AND DISCUSSION

### 4.1 Experimental Results

#### 4.1.1 Mass distribution of SEPT30 for modeling

Individual bacterial mass was normally distributed with a median of  $1.19 \pm 0.248$  pg (n = 14) (Figure 11).

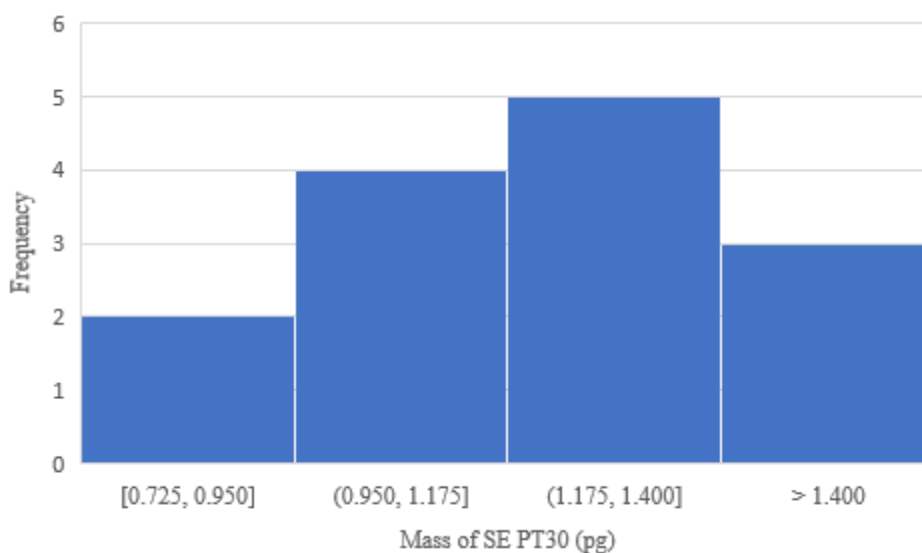


Figure 11 *Salmonella* Enteritidis PT30 mass measurements from methods described in Section 3.2 (avg mass = 1.19 pg and SD = 0.248 pg).

#### 4.1.2 SEM Imaging and Size Distribution Based upon Images

Figure 12 shows one of several (n=3) SEM images used to determine the dimensions of *Salmonella* Enteritidis PT30. The raw SEM images were processed using ImageJ to identify individual bacteria from the background, and the dimensions were measured using the reference scale, ROIs were selected at random without bias. Although the generic shape of *Salmonella* is a rod with rounded ends (i.e. a cylinder with two hemispheres), an elliptical sphere was used to approximate the dimensions with a major axis  $a$  and minor axis  $b$ , which was effective to

accounts for image variability while minimizing errors of measurements. Also, the circularity of the *Salmonella* was calculated (

Figure 13, Figure 14).

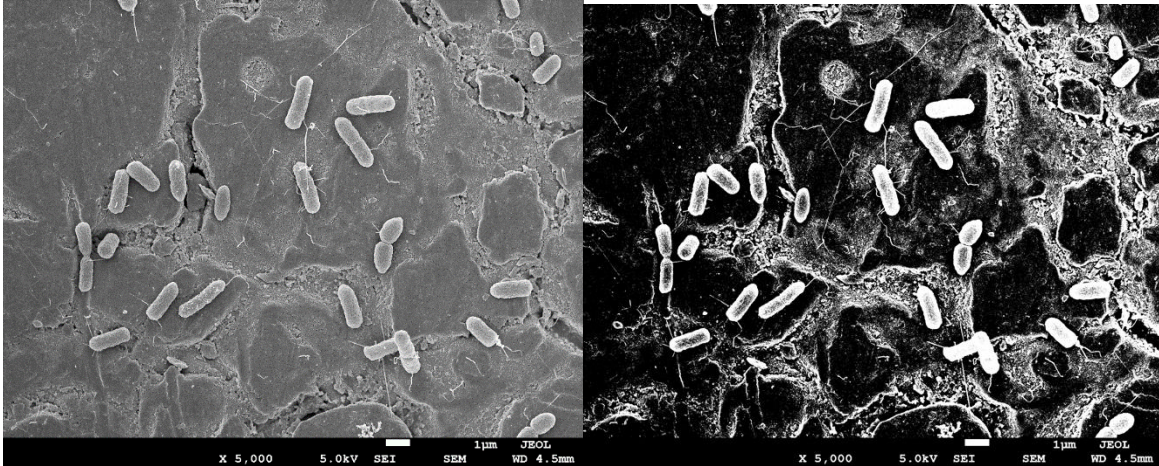


Figure 12 Original SEM image of *Salmonella* Enteritidis PT30 on stainless steel (304 #4 brushed finish) (left) and the processed image (right) using ImageJ, where the cells can be identified from the background for further image analysis.

In addition to measuring physical dimension, the SEM images confirmed that the inoculation method of this study was able to attach non-overlapping bacteria on the stainless steel coupon, which was a critical condition of the models describing attachment between the bacteria and the surfaces. Additional SEM images of the process are included in Appendix A.

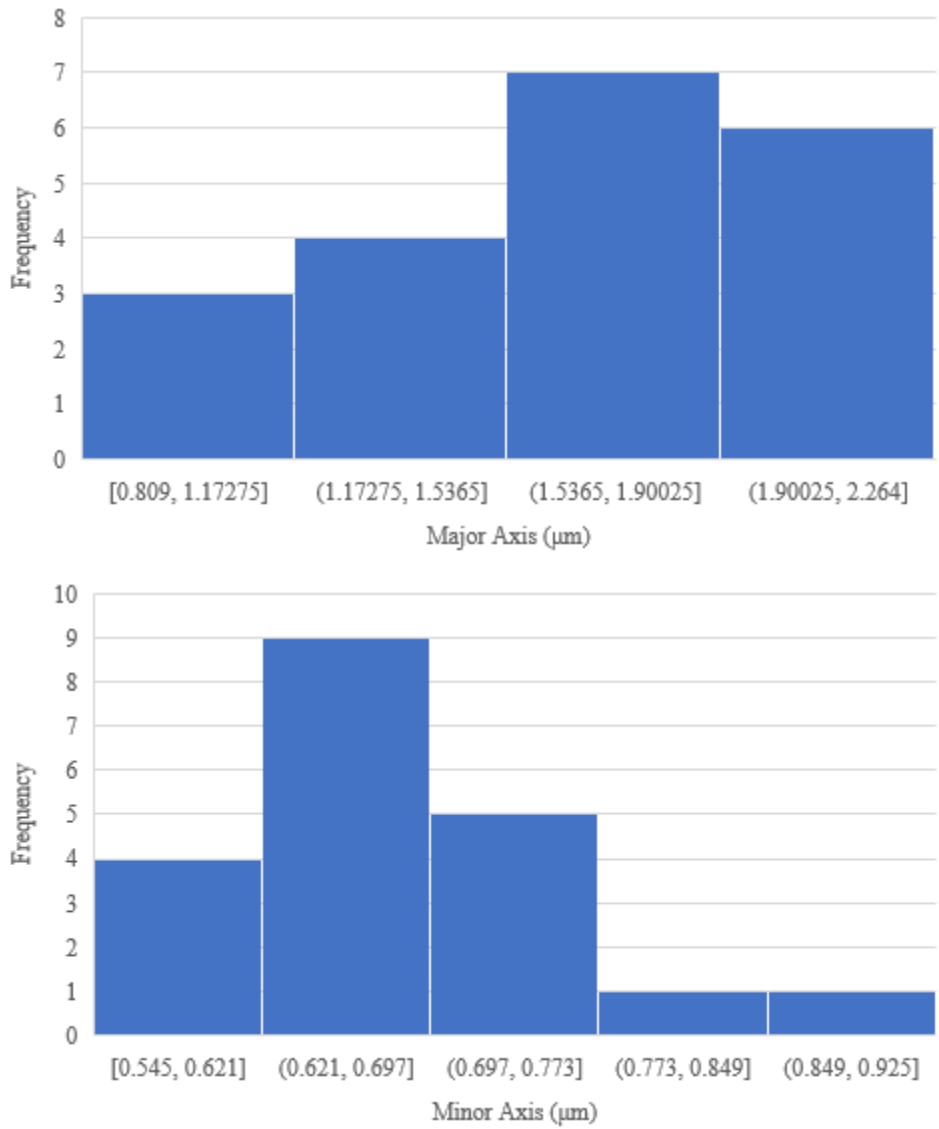


Figure 13 The distribution of the major and minor axis dimensions of *Salmonella* Enteritidis PT30 attached and desiccated on the surface of stainless steel.

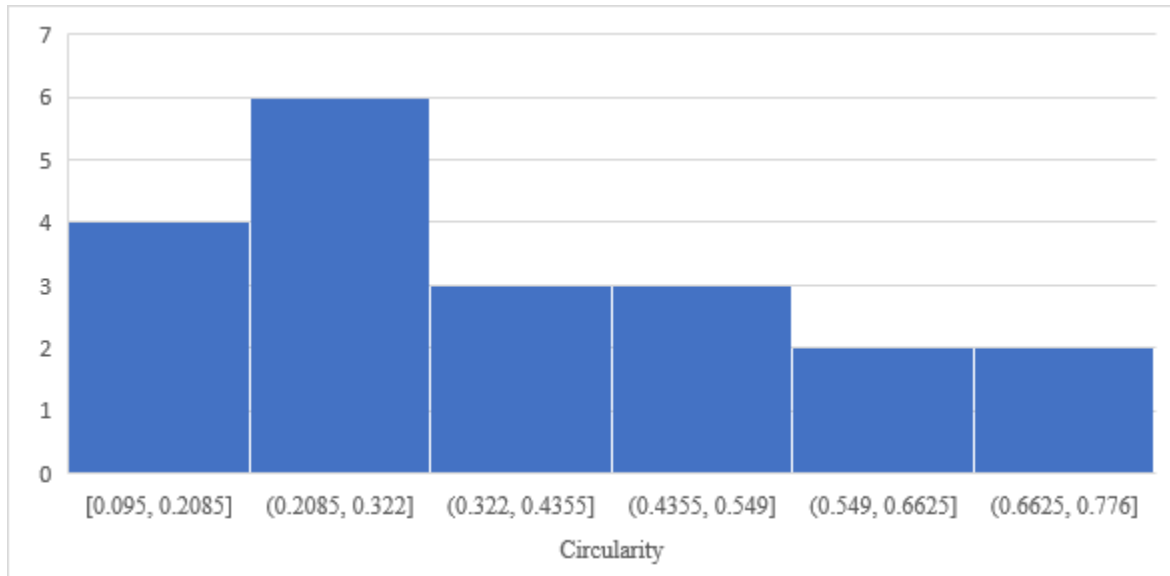


Figure 14 The distribution of the circularity (ellipsoid approximation) of *Salmonella* Enteritidis PT30 attached and desiccated on the surface of stainless steel.

Based on the histograms above, the circularity and minor axis dimensions of the bacteria followed a normal distribution, with a more uniform distribution of major axis sizes. The mean values and confidence intervals for each parameter are described in Table 1. The Shapiro-Wilk Normality test accepted the normality of the Major axis, Minor axis, and Circularity data ( $p > 0.05$ ).

Table 1 Mean and confidence interval values of the major axis, minor axis, and circularity of elliptical shape approximation for *Salmonella* Enteritidis PT30 on stainless steel surface.

<b>Dimensions/Parameter</b>	<b>Mean</b>	<b>CI (95%) (LL, UL) *</b>
<b>Major axis</b>	1.6624 ( $\mu\text{m}$ )	(1.456, 1.868)
<b>Minor axis</b>	0.6909 ( $\mu\text{m}$ )	(0.653, 0.729)
<b>Circularity</b>	0.3608 (dimensionless)	(0.271, 0.450)

\*LL: Lower Limit; UL: Upper Limit

From the SEM image analysis, the mean values, distribution trend lines and confidence intervals of the shape and size parameters of *Salmonella* Enteritidis PT30 were successfully quantified.

#### 4.1.3 AFM Imaging and Force Measurements

##### 4.1.3.1 Surface Properties

Using the Cypher AFM with a 300 kHz SiN tip (Figure 15) root mean square (RMS) roughness of the two different types of stainless steel was quantified over a 20  $\mu\text{m}^2$  area (Figure 16). The imperfections and inconsistencies of the materials were visually evident.

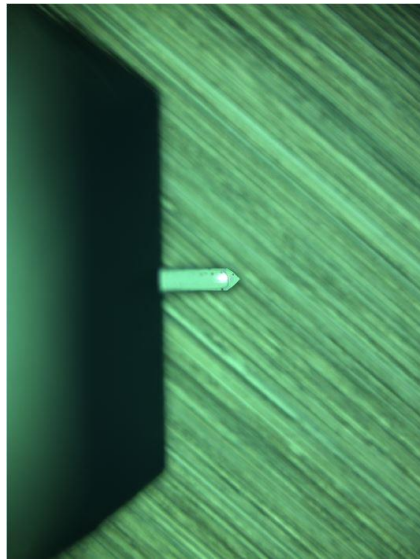


Figure 15 Optical microscope image of the Cypher AFM performing topographical measurements of the stainless steel #4 brushed finish using a 300kHz SiN tip.

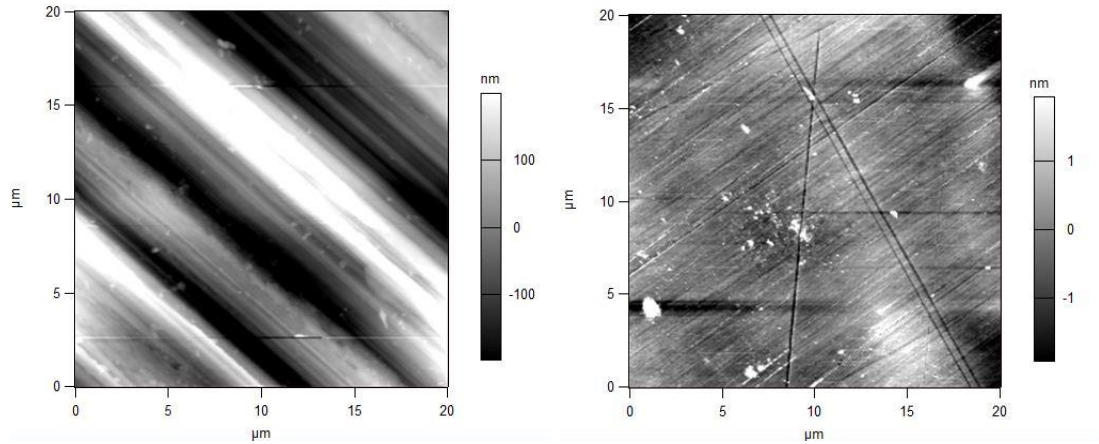


Figure 16 AFM Alternating Current (AC) topographical visualizations of stainless steel finishes #4 (left) and #8 Mirror (right), demonstrating a noticeable difference in surface roughness.

Table 2 Root Mean Squared (RMS) surface roughness for each stainless steel finish type.

Material	RMS Roughness	Max Peak Height $\Delta$	Max Peak Width $\Delta$
SS304 #4 brushed	138.310 nm	453.210 nm	1.573 $\mu\text{m}$
SS304 #8 mirror	0.974 nm	1.0160 nm	47.159 nm

Clear differences were measured between the materials (Figure 18). Based on the minor axis dimensions from the SEM images, the width of the brushed pattern in the #4 finish coupon is wide enough for bacteria ( $\sim 1 \mu\text{m}$ ) to be strongly attached to the surface due to the increased contact area.

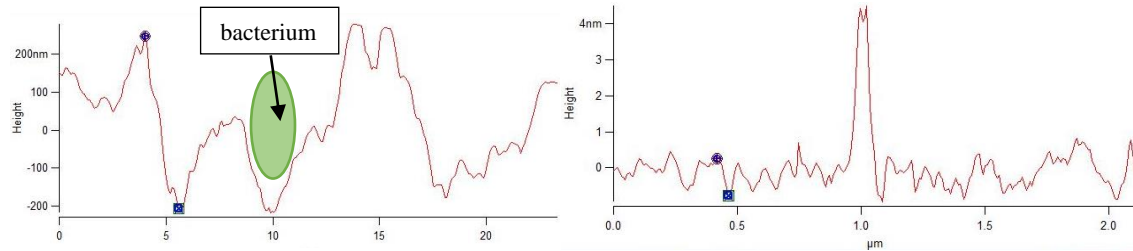


Figure 17 Height retrace from AFM of stainless steel 304 #4 brushed (left) and #8 Mirror (right) to determine the average surface roughness (RMS).

#### 4.1.3.2 *Salmonella* Properties

*Salmonella* was evenly dispersed on the surface as visually confirmed by SEM, and imaged using the Alternate Current (AC) topographic method, similar to the measurement for the stainless steel roughness.

The topographic method can image individual bacterial cells desiccated on the surface with no modification, a distinct advantage to the SEM imaging techniques where samples must be prepared in glutaraldehyde solution for imaging, leading to possible distortion. Figure 18 shows that the individual cells on the surface are similar in size for both AFM and SEM images, indicating that desiccation does not significantly alter the physical dimensions of *Salmonella* despite the loss in water.

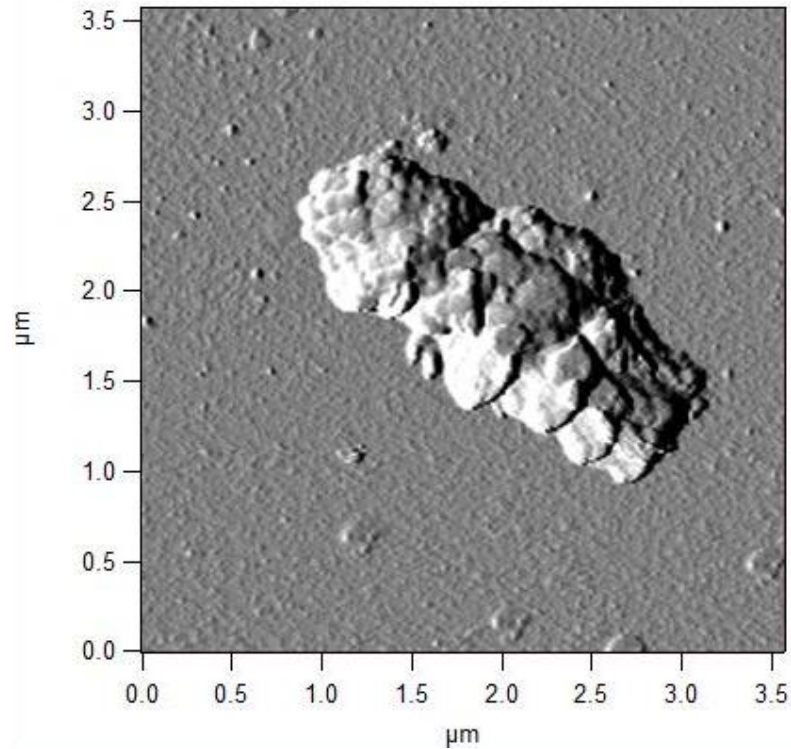


Figure 18 AFM image of desiccated a *Salmonella* cell on stainless steel #8 finish (AC Topographical mode of Cypher AFM with 300 kHz Silicon Nitride (SiN) fine point tip).

After imaging *Salmonella*, the Au coated PNP tipless cantilever was used for force mapping the location of the individual cells. Based on a  $20 \mu\text{m}^2$  area where *Salmonella* is most present on the surface, a force mapping divided the region into N points, where the AFM can generate force extension and retraction curves. The amount of deflection of the cantilever required to completely retract from the surface was calculated as the adhesion force by the spring constant of the cantilever, a known value of the geometry of the cantilever ( $k = 0.02 \text{ N/m}$ ).

Force mapping showed a distinct difference between the biomass on the surface and the stainless-steel surface alone (Figure 20). Based on the extension and retraction curves of the cantilever interacting with the materials, clear differences between interactions were seen for the

bacteria and the cantilever and the stainless-steel surface. The adhesion force was interpreted as the maximum force occurred from the retraction of the cantilever (blue line) (Figure 21).

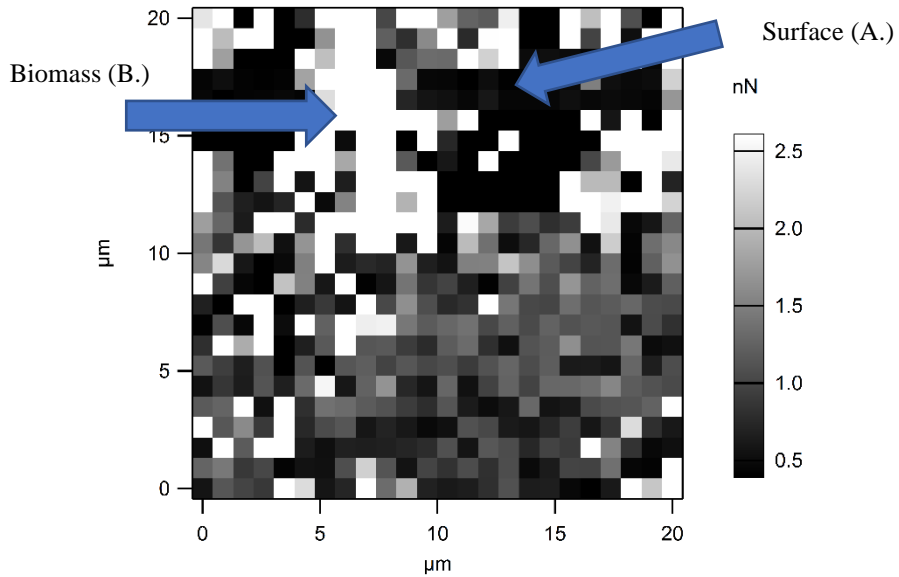


Figure 19 Force Mapping of *Salmonella* and stainless steel showing high force areas (white) are where bacteria is located, low force areas (black) is the surface, where little interaction occurs.

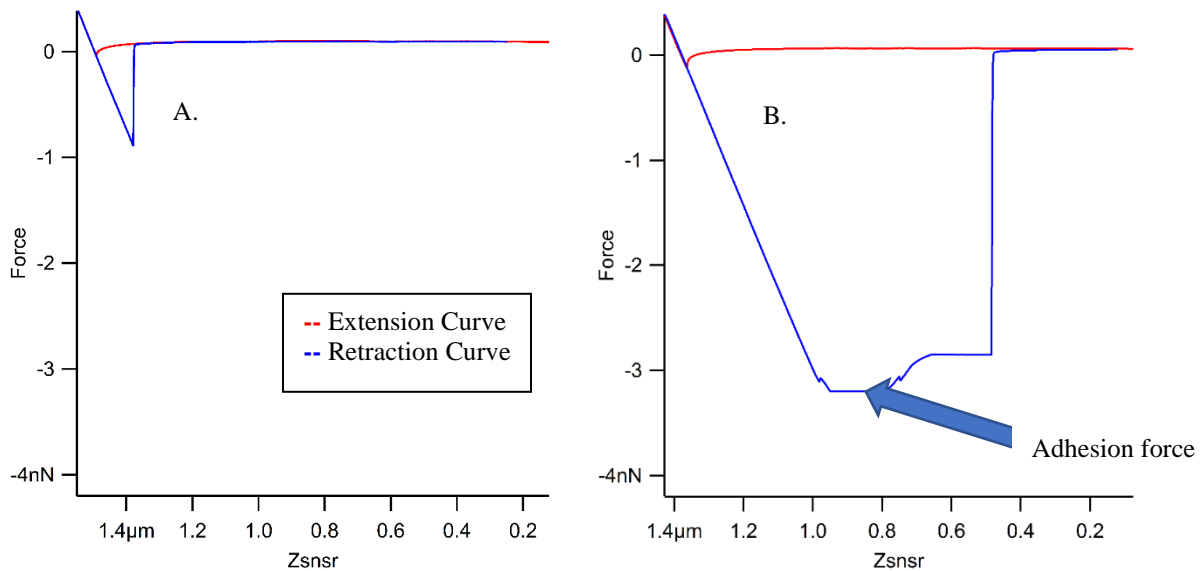


Figure 20 Interaction force between stainless steel and cantilever (A.), and the *Salmonella* and the cantilever (B.). Retraction from the surface is deflected based on the adhesion force interacting with the cantilever and the surface.

After a force mapping a  $20 \mu\text{m}^2$  region, a histogram of maximum adhesion forces was generated (Figure 21), which shows the clear difference of adhesion force values for the surface (values near zero) and the *Salmonella* (large values above 3.0 nN). Artifacts of data inside the histogram are values measured near the edges of the biological material, and any other deposits on the surface. Confirmation that the recorded adhesion value is associated with the *Salmonella* and surface was referenced by the respective height mapping of each measurement value, for example, an adhesion measurement of 3.5 nN occurred at a height map of  $0.5 \mu\text{m}$ , where was a measurement close to 0 nN was at a height map of  $0 \mu\text{m}$ .

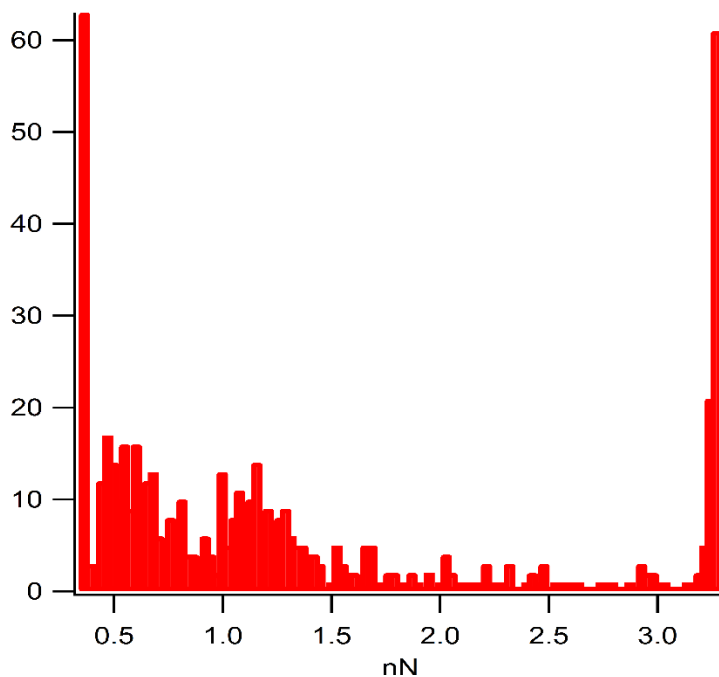


Figure 21 Histogram of maximum adhesion force from AFM force mapping of cantilever-surface (near zero points) and cantilever-*Salmonella* ( $\sim >3.0$  nN).

To verify the magnitude of the adhesion force, *Salmonella* was attached to the cantilever using cyanoacrylate (see Sec. 3.4) after which extension and retraction forces were measured by placing the cantilever near clear stainless steel surface.

Force mapping measurements of the cantilever with bacteria attached was assembled into a histogram (Figure 22, A). Thereafter, a force mapping was performed over areas of the stainless steel with attached *Salmonella* to assess any difference with *Salmonella-Salmonella* force measurements (Figure 22, B). The two histograms show a large sampling of *Salmonella*-surface interaction, and *Salmonella-Salmonella* interaction, with the measured maximum adhesion force of 3.405 nN and 3.157 nN, respectively.

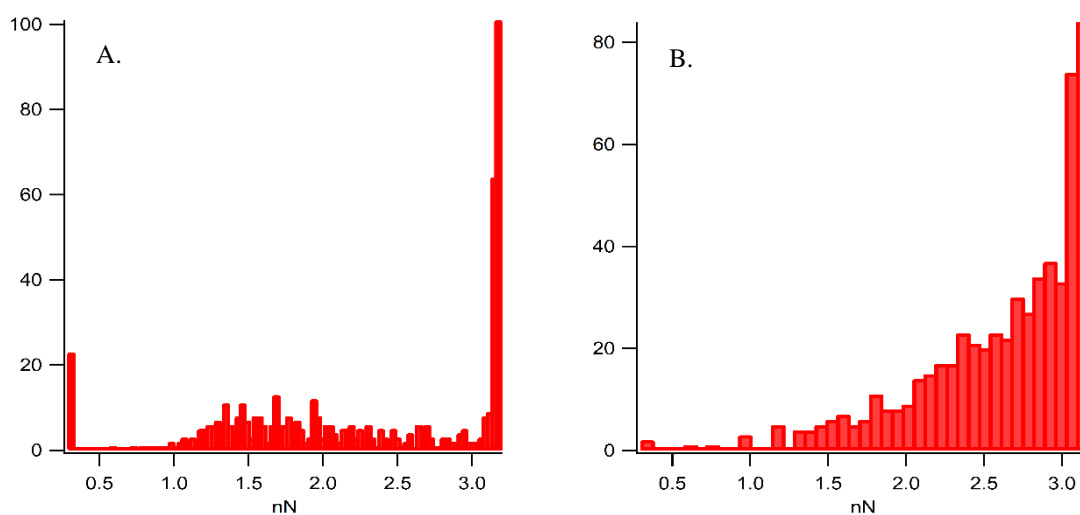


Figure 22 Histogram of maximum adhesion forces for: (A) *Salmonella* interacting with a stainless steel surface; (B) *Salmonella* attached to a cantilever interacting with *Salmonella* on stainless steel surface.

The *Salmonella*-surface force mapping data was truncated to values greater than 3.25 nN for statistical analysis as the bacterial adhesion force to the stainless-steel surface. The cut-off value of 3.25 nN was chosen as the beginning of the normal distribution of forces related to the bacterial adhesion, and determined by referencing the height mapping of all respective values where *Salmonella* was present. Thus, the estimated adhesion force,  $F_{ad} = 3.3459 \pm 0.0283$  nN (n=330), was utilized for further modeling implementations.

Also, Cypher AFM’s interfacing computer program was able to utilize force mapping data to fit the indent Young’s modulus ( $E_c$ ) utilizing a weighted ordinary least squares algorithm (internal to Cypher AFM). The Young’s modulus of the bacteria, which is related to the amount of deformation of the bacteria when a certain force is applied, was calculated to 67.26 kPa (Table 3). However, Cypher AFM did not report confidence intervals of the parameter estimation. The Young’s modulus ( $E_2$ ) of stainless steel was 290 GPa which was four orders of magnitude higher than that of *Salmonella*. Also, the average JKR contact area was  $0.475 \mu\text{m}^2$ . Cypher AFM selected the Poisson ratios ( $\nu_1, \nu_2$ ) of the materials without user submission. Bacterial adhesion measurements were only performed on #8 mirror finished stainless steel 304.

Table 3 Cypher AFM calculated Young’s modulus and JKR contact area of desiccated *Salmonella* Enteritidis PT30 on stainless steel surface.

Properties	Values	Units
Indent $E_c$ (Bacteria)	67.26	kPa
Indent $V_1$	0.33	N/A
Indent $V_2$	0.25	N/A
Indent $E_2$ (Stainless Steel)	290.0	GPa
JKR Contact Area	0.474976	$\mu\text{m}^2$

#### 4.1.4 Centrifuge Experiment Results

Microscale measurements of *Salmonella* properties provide a fundamental understanding of the mechanics of adhesion and detachment. However, considering individual variation in

*Salmonella*, statistically valid number of observations is impractical to realize large scale implications of contamination. Therefore, in an attempt at first understanding the empirical observation of detachment with a laboratory centrifuge would provide a more statistically reasonable quantification of bacterial adhesion on stainless steel surfaces. With uniformity (i.e., non-overlapping cells) of the inoculation method confirmed by the SEM images, the samples once placed in the holder, with the end sample surface being normal to the centrifuge (for SS-34 holder 34° from the axial plane) to the centrifugal force, provided a proper detachment force experimental design.

Stainless steel samples of both #4 and #8 finish were initially subject to a 5000 RPM (2988 ×g RCF) treatment for 5 min. For the #8 mirror finish stainless steel samples, a statistically significant ( $p < 0.05$ , Student's t-test) difference was observed between the positive control and the sample spun at 5000 RPM (2988 ×g RCF), with an average 0.79 log(CFU/cm<sup>2</sup>) reduction in *Salmonella* on the surface (Figure 23). However, there was no significant difference between the control and treated samples for #4 finish. This result agrees well with the analysis of the surface roughness (Sec 4.1.3.1) which increases surface attachment potential of the *Salmonella* for #4 finish compared with #8 mirror finish. Thus, #4 finish stainless steel surface requires more centrifugal force to remove *Salmonella* from a rough surface as opposed to a uniformly flat surface.

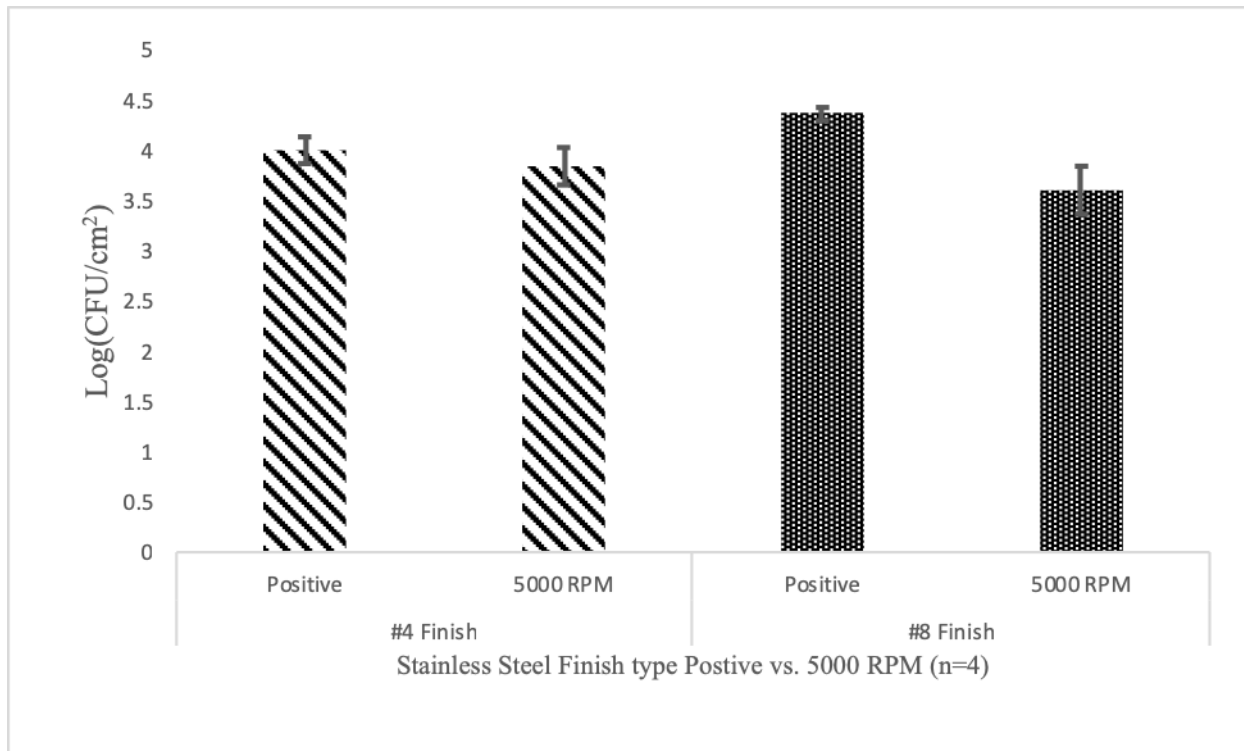


Figure 23 Critical attachment force measurements for *Salmonella* Enteritidis PT30 attached on stainless steel coupons (#4, and #8 finish), the positive (control, 0 RPM) and the samples centrifuged at 5000 RPM (treated, 5000 RPM).

After the comparison test, data points for #8 mirror finish stainless steel were collected at 300, 1000, 4000, 5000, and 10000 RPMs (n=3). The general trend for #8 finish indicates that there exists strong evidence for the distribution of the attachment forces (~90% detachment at 4000 RPM, Figure 24). The RCF of the centrifuge at 4000 RPM was  $1912.3 \times g$ , with an average mass of 1.19 pg for a single cell of *Salmonella*, which corresponds to an average pull off force of 22.3 nN. Many occurrences of experimental errors lead to many data points were not in agreement with individual measurements, and even at 10000 RPM, there was still no significant difference in bacteria concentration for the #4 Finish stainless steel. The operation of the

centrifuge over 10,000 RPM were not performed due to the risk of equipment failure. Further improvements to the experimental design could be performed by development of systems capable to exceed the limits of the centrifugal force or more abrupt force interactions.

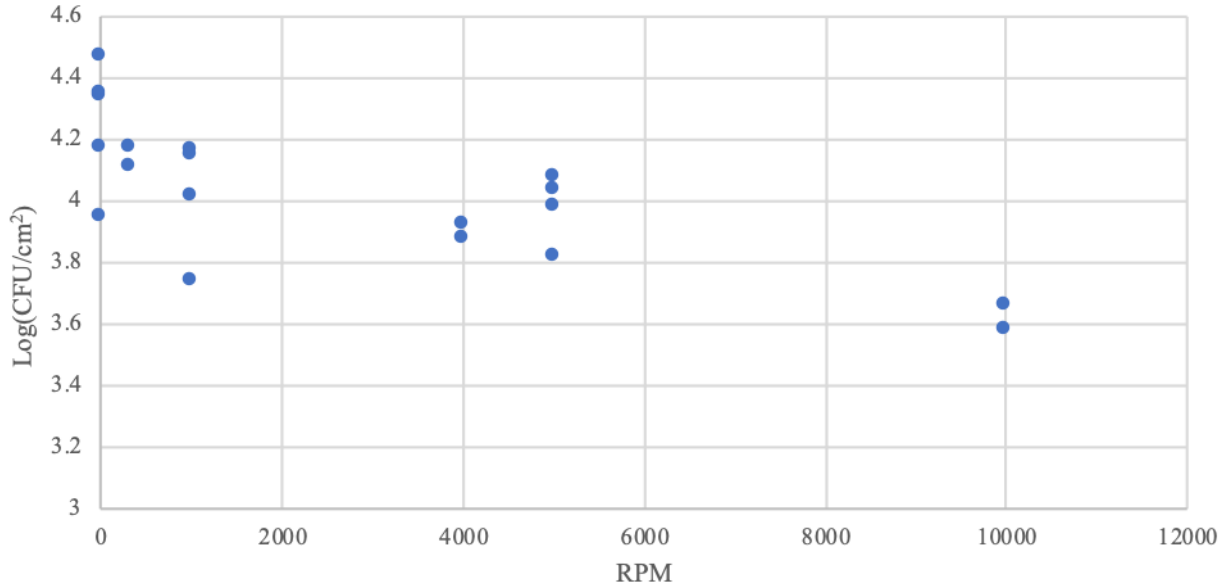


Figure 24 The remaining population (Log(CFU/cm<sup>2</sup>)) of desiccated *Salmonella* Enteritidis PT30 attached to stainless steel (#8 finish) after centrifugation at 300, 1000, 4000, 5000, and 10000 RPM

## 4.2 DEM Modeling

Due to the experimental measurements of the critical bacterial attachment forces and the relevant properties, the first principle-based DEM model capable for industrial scale-up application, was successfully developed and validated.

### 4.2.1 DEM Modeling and Visualization

By dividing of the average force of adhesion by the contact area (Sec. 4.1.3), the surface energy density,  $k$ , was estimated at 6947 J/m<sup>3</sup>. The simulation was run over a force range of 0 nN to 10 nN applied to each particle in the positive Z axis. Starting with 150 model *Salmonella* cells

deposited to the surface, the remaining cells on the surface was enumerated as the pull off force increases (Figure 25).

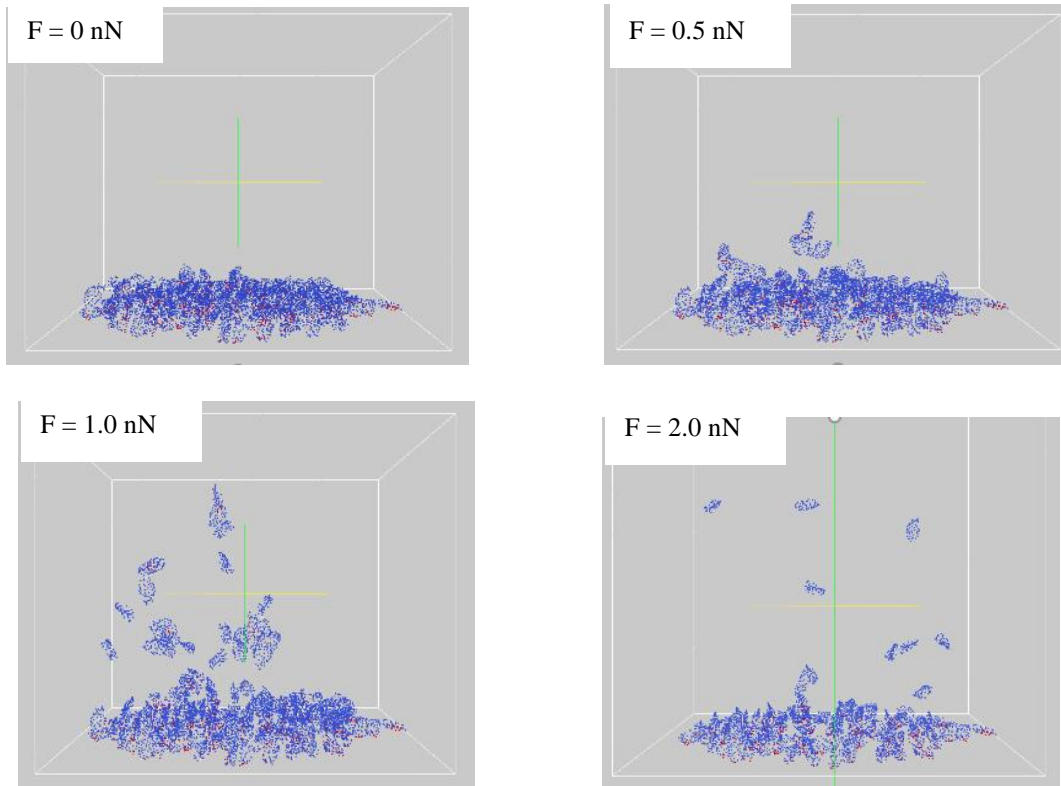


Figure 25 Detachment of the multi-spherical model bacterium from the surface with an increasing pull off force in the +Z direction (upward).

The Detachment of the *Salmonella* did not occur all at one discrete force value, but rather over a range of forces individual and conglomerated groups of bacteria began to release from the surface. This occurred because not all particles were evenly deposited to the surface with even contact area, however, this would be comparable to real life situation. All sporadic detachment events occurred well below the measured adhesion force until the number of bacteria was left remaining on the surface with every particle removing itself equally at a value of 3.821 nN (cf.  $F_{ad} = 3.3459 \pm 0.0283$  nN (n=330) from AFM force mapping). The simulation data recreates a

real-life scenario with observed variance similar to empirical expectations. These findings show that the adhesion pull off force is the limiting value of concern for complete particle removal from a surface with maximum surface contact area (Figure 26). This is the first step to further understanding the first principle interactions involved with the detachment process of bacteria.

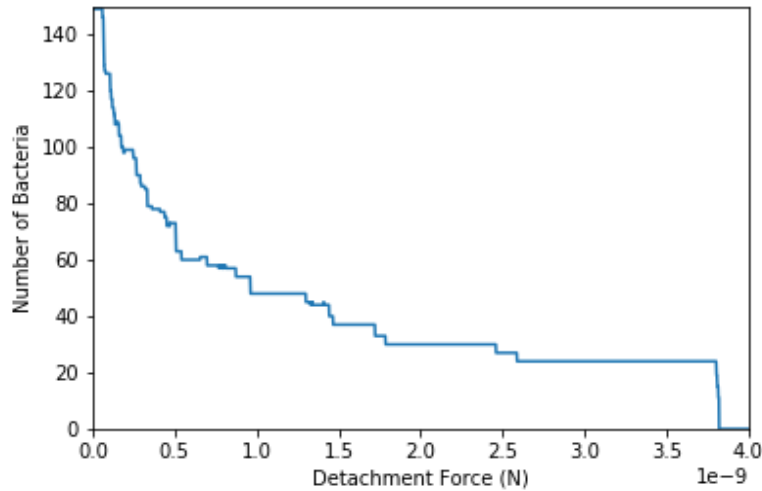


Figure 26 Integer number of model bacteria remaining attached to a surface as a linear increase of detachment force.

#### 4.2.2 Monte Carlo Modeling Based upon Fundamental Properties

Validation of the first principle based simulation agreeing with individual bacteria measurements confirms the usefulness of the JKR theory to the phenomena of bacterial adhesion in low-moisture environments. Combining the individual bacteria results and theory implementation to further interpret the canonical centrifuge results from Section 4.1.4 would further validate the explanation of certain adhesion results from other empirical experiments.

The results of the Monte Carlo simulation show a similar trend line with the experimental results using centrifuge (Figure 27), and the optimized surface energy density was  $W = 4658.201 \pm 105.320 \text{ J/m}^3$  (RMSE = 8812 CFUs) which deviates from the AFM result by approximately 33%. However, the estimated surface energy density is well within the order of magnitude of

measurements considering inherent errors, such as the increasing confounding variables found in experimental data, experimental errors, or contributions from more parameters than just the initial surface energy density. As expected, the Monte Carlo simulation reached zero CFUs on the surface, whereas the experimental results never reached zero in Figure 27.

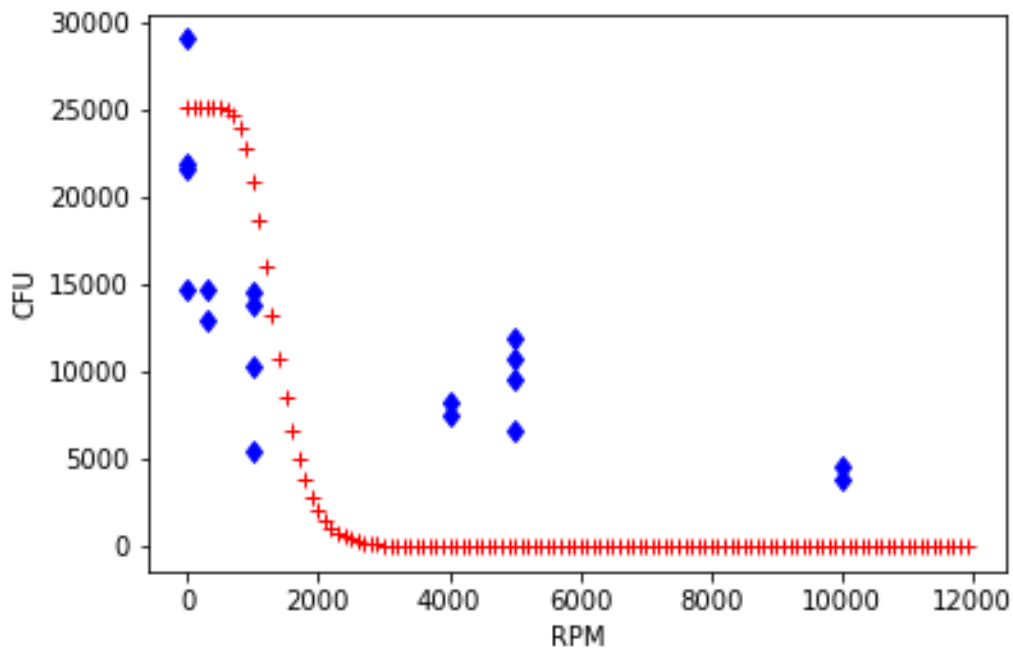


Figure 27 Experimental data (blue diamond symbol) vs. Monte Carlo modeling data (red cross symbol) for attachment force (via centrifugal force) distribution of *Salmonella* Enteritidis PT30 to stainless steel surface in low-moisture environment.

### 4.3 Summary

Overall the objectives of this study have been achieved as explained above which can be summarized as follows:

- 1) Parameters concerning bacteria dimensions, and mass were measured directly.
  - a) SEM images of bacteria desiccated on a stainless-steel surface indicate no physical decrease in dimensions as a function of moisture.

- b) AFM measurements of adhesion force, Young's Modulus, and contact area were obtained for *S. Enteritidis* PT30 in a low-moisture environment
- 2) The experimentally measured bacteria properties were implemented to the DEM model by utilizing the JKR theory, providing a fundamental understanding of the kinematics of bacterial adhesion.
  - 3) Statistical quantification of adhesion force by the centrifugation experiment provided macroscale results about the detachment of *Salmonella* Enteritidis PT30 from stainless steel surfaces.
  - 4) A Monte Carlo algorithm was developed to implement the JKR theory to explain large scale empirical results regarding bacterial adhesion to stainless steel surfaces.

#### **4.4 Discussion**

Under current experimental conditions, it was challenging to achieve 100% removal of bacteria from the surface; this may indicate that a portion of the population is irreversibly attached and requires a much higher order of magnitude of force to detach, and more model parameters must be considered to accommodate all empirically found results.

However, using SEM imaging and AFM techniques, fundamental data was measured and used in DEM modeling which effectively validated the microscale measurements. Generally, large scale experimental results are not always consistent, all factors are not known, and direct observation is nearly impossible (a common case for most microbiological experiments). Therefore, incorporating the first principle based models to describe phenomena such as adhesion not only provides a more direct incorporation of parameters, as opposed to large uncertainty practices, but it also has the distinct advantage of being scaled to any dimension of low-moisture environments, because the model is developed based upon the first principle

kinematics with fundamental properties. The framework of micro-scale measurements and simulation to elucidate a large scale phenomena such as cross-contamination is only as good as the validation approach. Thus, the objectives of this study was to provide an initial attempt at first principle based modeling techniques of individual bacterial adhesion to industrial equipment surfaces, such as stainless steel. With the further addition of large-scale experimental validation and Monte Carlo simulation from obtained measurements would help correlate the micro-scale model to a large scale empirical result. In addition, if the Monte Carlo experimental results could be implemented with better resolution and accuracy, a method would be available for researchers to obtain fundamental measurements such as the force of adhesion of any microorganism of concern with high confidence.

Most bacterial adhesion studies have used in solution measurements to implement DLVO theories for understanding the work of adhesion to the surface and liquid interfaces (Hermansson, 1999; Hori & Matsumoto, 2010; Huang et al. 2015), which makes comparison to desiccated results impractical. Although Huang. et al. reported an adhesion force of  $-3.0 \pm 0.4$  nN of *E. coli* and goethite submerged in water (Huang et al. 2015), no specific strain, or different adhesion parameters were mentioned.

In this study for desiccated bacteria, the conditioning of the bacteria on the sample surface at 45% RH was chosen as a nominal ambient condition similar to a processing facility. Because the measurements of adhesion force, amount of bacteria detached, and dimensions of the bacteria can be significantly affected by the relative humidity of an environment, the effect of humidity on the results needs to be investigated.

## **CHAPTER 5. CONCLUSIONS**

### **5.1 First Principle Based Modeling**

“All models are wrong, but some are useful” George Box said (Burnham & Anderson, 2010). Minimizing a number of assumptions as inputs to a model improves efficiency, accuracy, and leads to the further discovery of scientific openings. The equally feasible black-box modeling approaches such as parametric regression lack the ability to scale to other use-cases without validating the assumptions of the models, first principle based modeling strives to eliminate this. Microbiology, where microbes are too small to measure, many canonical and empirical results are used to deduce specific mechanisms. Utilizing computational tools such as LIGGGHTS, precision measurement tools, and discrete modeling techniques, complex phenomena, such as dry cross-contamination and bacterial adhesion, can be elucidated further.

### **5.2 Suggestions**

The objective of implementing a first principle-based model of bacterial adhesion was met. Further development and validation of the model would provide more accurate parameter estimations with more statistically sound models. The initial justification for a first principle-based model was to further understand large scale cross-contamination events. Understanding the force required to detach bacteria at the micrometer scale can be easily implemented to DEM models with theoretically full accuracy, in turn observing the propagation of bacteria in a large-scale system such as an almond processing line with less cost and experimental involvement of introducing pathogens to the environment. Future work would be to scale the DEM simulations to industrial scale environments, such as a large-scale almond processing line, complete with food debris and kinematic interactions of the product, bacteria, and processing equipment. The

potential to model the distribution of a contamination event or the efficacy of specific low-moisture sanitation procedures by the required detachment force of bacteria has many benefits as opposed to empirical tests. Farakos et al. discussed the impact of cross-contamination events in almond processing on the quantitative risk assessment in junction with microbial treatments (Farakos. et al. 2017), a further fundamental understanding of the cross-contamination in a large-scale environment would help accurately determine the relative risk associated with specific process methods and equipment.

In addition, the DEM modeling of bacterial adhesion is not a common skill set in microbiological laboratories. Therefore development of a Monte Carlo model to understand the bacterial adhesion at a large-scale event, can provide an efficient methodology for the microbiological community to obtain parameters such as work of adhesion for different organisms in low-moisture environments. If a Monte Carlo model can determine the additional factors contributing to adhesion and be modeled with empirical data efficiently, physiological behaviors could be observed for different pathogens. This fundamental information for adhesion of pathogens in a low moisture environment would help elucidate the persistence and assist in bacterial removal techniques for further research in food process equipment safety.

## **APPENDICES**

## APPENDIX A. Scanning Electron Microscopy Images

Samples were processed and images were taken at Michigan State University's Center for Advanced Microscopy (CAM) in the College of Natural Sciences. JEOL 7500F SEM, equipped with Scandium image processing software by Olympus Soft Imaging Solutions, was used. The images below are all supporting the hypothesis of even distribution of *Salmonella* across the surface, and used for size measurements as well.

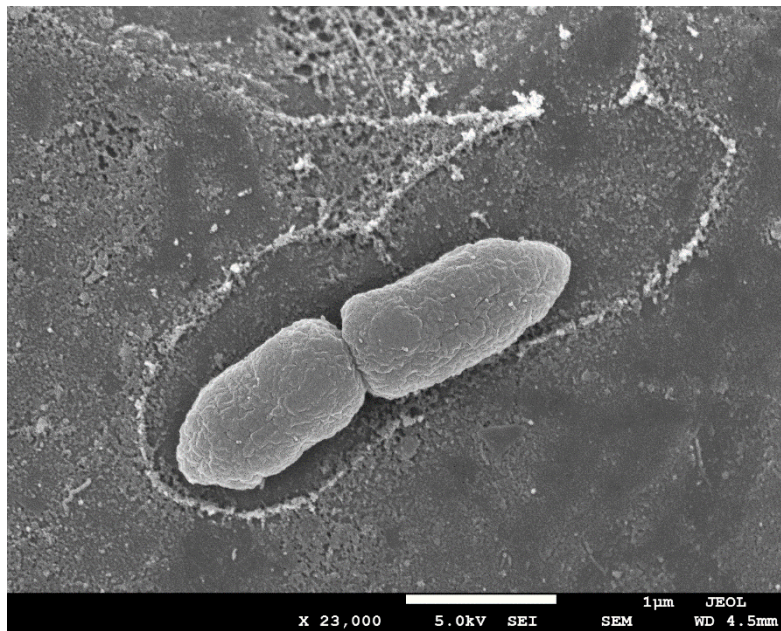


Figure 28 Initial moisture ring observed around the individualized *Salmonella* Enteritidis PT30 on stainless steel from SEM imaging.

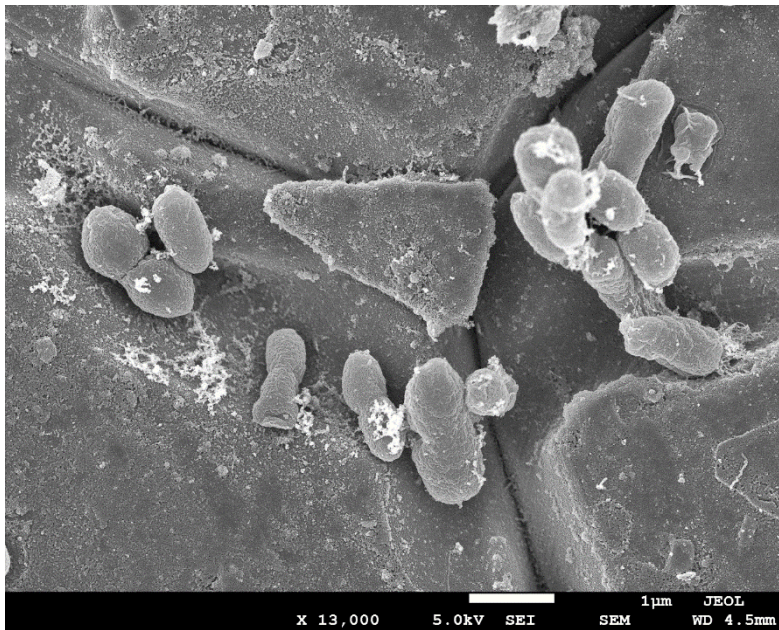


Figure 29 Conglomerates of *Salmonella* Enteritidis PT 30 harbor around grooves of the metal, #4 surface finish, increasing contact area with surface, significantly increasing the amount of force required to remove the bacteria.

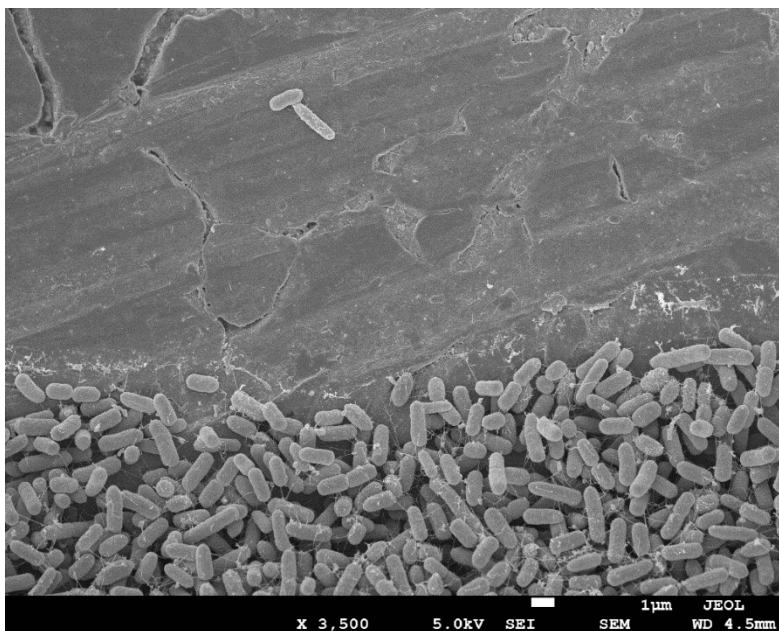


Figure 30 High concentrations of *Salmonella* deposited on the surface of stainless steel creates a dense multiple layer environment for the bacteria, indicating that initial concentration of bacteria directly effects the contact area and surface energy associated with adhesion of bacteria.

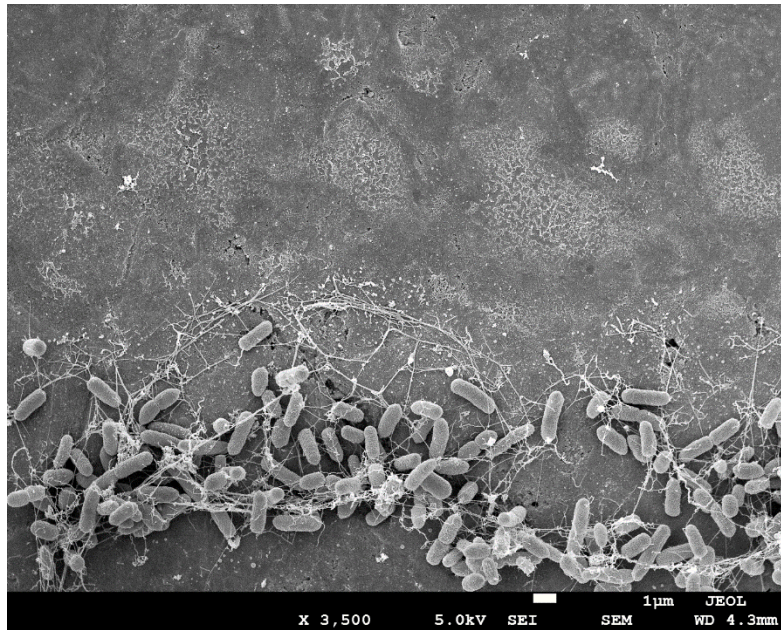


Figure 31 Remnants of the flagella and ECM from *Salmonella* Enteritidis PT30 can still survive the desiccation process if the inoculation level is high, further increasing adhesion to surface.

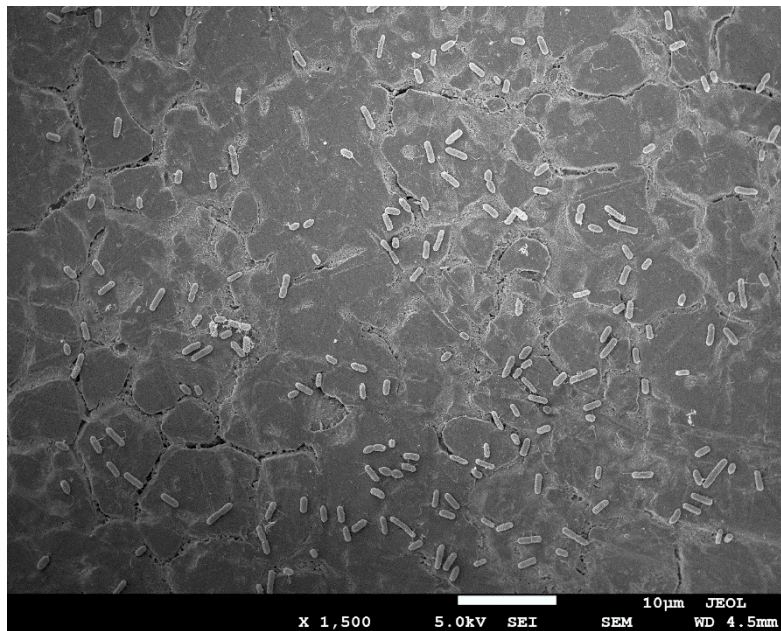


Figure 32 #8 Mirror finish stainless steel was adequate for generating non-overlapping *Salmonella* Enteritidis PT30 on surface smooth enough not to trap bacteria in between the grain boundaries of the metal. This conclusion is important for the modeling of individual bacteria to detach off surface given an imposed force.

## APPENDIX B. Atomic Force Microscopy Data

The Cypher™ Atomic Force Microscope/Scanning Probe Microscope, is located with the Michigan State University Department of Physics and Astronomy's Condensed Matter Physics group. With an internal data processing program, capable of performing height mapping, force mapping, and parameter estimation of properties, the Cypher™ AFM can perform measurements up to nm resolution. Below are supporting images acquired during testing.

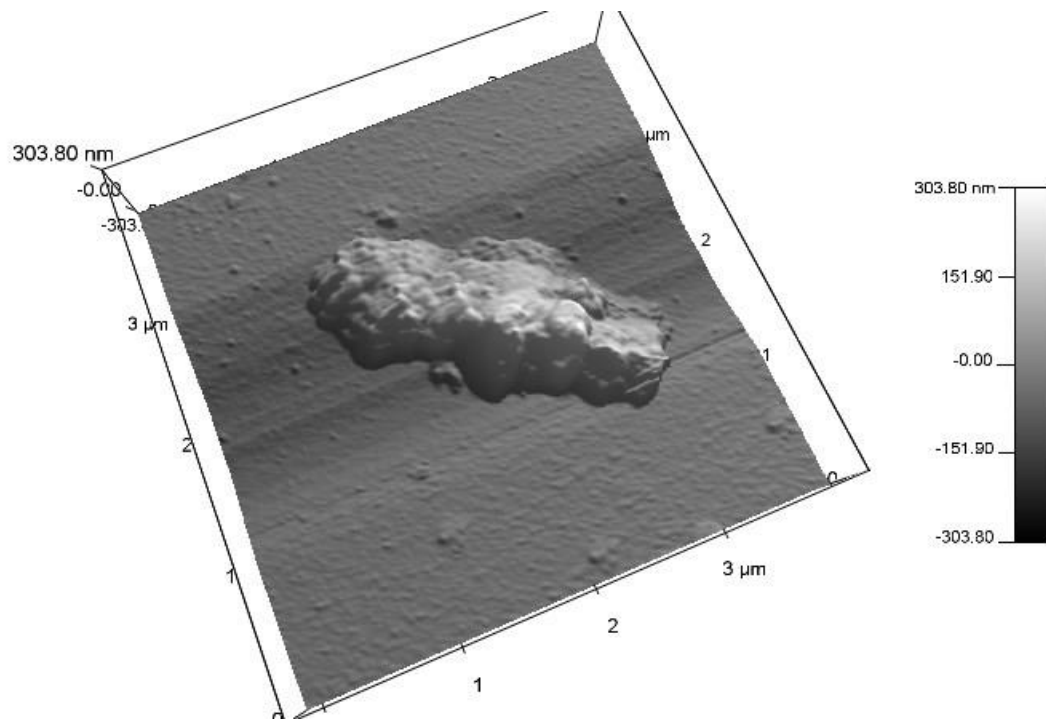


Figure 33 3-dimensional height retrace of individual *Salmonella* on surface, the Cypher AFM has the capability of reaching very small dimensions while measuring (~nm scale), showing individual roughness, and direct interaction with the bacteria in a physical state.

## APPENDIX C. Modeling Code

Several scripts were used to perform modeling analysis. Installation of LIGGGHTS and DEM resources can be found at [www.cfdem.com](http://www.cfdem.com). LIGGGHTS is a Command Line Interface (CLI) program, that requires an input script of physical parameters of the model (listed below). The output are particle specific coordinate, velocity, and acceleration information at each specific timestep which can be analyzed by post process scripts. Monte Carlo simulation scripts of the centrifuge experiment is listed below as well.

### LIGGGHTS DEM CODE

```
#Multisphere

atom_style granular
atom_modifymap array sort 0 0
boundary      m f
newton                off

communicate single vel yes

#PUBLIC version only supports serial execution
processors 1 1 1

units          cgs

region          reg block -.00225 .00225 -.00225 .00225 -0.0001 .05 units
box
#region          reg1 block -.00125 .00125 -.00125 .00125 0.005 .01 units
box

create_box 2 reg

neighbor 0.0004 bin
neigh_modify      delay 0

#Material properties required for new pair styles

soft_particles yes
fix          m1 all property/global youngsModulus peratomtype 6.7e5 1.e7
fix          m2 all property/global poissonsRatio peratomtype 0.45 0.45
fix          m3 all property/global coefficientRestitution peratomtypepair
2 0.3 0.3 0.3 0.3
fix          m4 all property/global coefficientFriction peratomtypepair 2
0.5 0.5 0.5 0.5
```

```

fix          m5 all property/global characteristicVelocity scalar 2.
#fix         m6 all property/global cohesionEnergyDensity peratomtypepair 2
69473 69473 69473 0
fix          m6 all property/global cohesionEnergyDensity peratomtypepair 2
694730 694730 694730 0
#New pair style
pair_style gran model hertz tangential history cohesion sjkr #Hertzian
with cohesion
pair_coeff * *

#1e-8

timestep    0.00000001

fix         gravi all gravity 980.665 vector 0.0 0.0 -1.0

fix zwalls all wall/gran model hertz tangential history cohesion sjkr
primitive type 2 zplane 0.0

#distributions for insertion
fix         pts1 all particletemplate/multisphere 15485863 atom_type 1
density constant 1.0 volume_limit 1e-13 nspheres 7 ntry 1000000 spheres
file data/bacteria.multisphere scale 0.0000328 type 1
fix         pddl all particledistribution/discrete 15485867 1 pts1 1.0

#region and insertion
region      bc cylinder z 0.0 0.0 .0020 .0005 .001 units box

fix         ins all insert/pack seed 32452843 distributiontemplate pddl
vel constant 0. 0. -1. &
            insert_every once overlapcheck yes region bc ntry_mc 10000
particles_in_region 150

#integrator for multisphere rigid bodies
fix         integr all multisphere

#output settings, include total thermal energy
compute     1 all erotate/sphere
fix         ts all check/timestep/gran 1000 0.1 0.1
thermo_style custom step atoms ke c_1 f_ts[1] f_ts[2] vol
thermo      1000
thermo_modify lost ignore norm no

#region      reg1 block -.00125 .00125 -.00125 .00125 0.005 .01 units
box

#insert the first particles so that dump is not empty
dump        dmp all custom 1000 post_multi/dump*.multi id type mol x y z
vx vy vz fx fy fz omegax omegay omegaz radius

#insert particles
#run        90000 upto
run         500000 upto

```

```

#run          5000 upto

variable fv equal vdisplace(0,0.1)
#variable fv equal vdisplace(0,1)
fix ff all addforce 0.0 0.0 v_fv
#run
#run 1700000 every 10 "delete_atoms region reg1 compress yes"
#run 1700000 every 100

run          3000000 upto
#delete things that exit the simulation

```

## LIGGGHTS POST PROCESSING PYTHON CODE

```

import numpy as np
import csv
import matplotlib.pyplot as plt

def slice(xpos, ypos, zpos, delta_x, delta_y, delta_z, d):

    j = 0
    i = 0
    p = len(d)
    for i in range(1,p):
        if(d[i,3] <= xpos+delta_x and d[i,3] >= xpos and d[i,4] <= ypos +
delta_y and d[i,4] >= ypos and d[i,5] <= zpos +delta_z and d[i,5] >=
zpos):
            #If the particle is inside the voxel, tally
            j+=1

    amount = j
    #Return the Average and standard deviation in each voxel
    return float(amount)
    #return False

xpos = -0.00125
ypos = -0.00125
zpos = 0.0
delta_x = 0.025
delta_y = 0.025
delta_z = 0.00025

ts = 0.00000001
particles_per_bact = 7
#Force is increased linearlly every timestep. (originally in Dynes, (1e-5
N)) in the Z direction
#due to the cohesive force, particles will stay until the force is greater
than adhesion
data = []
linear_force_displacement = 0.005*1e-5

```

```

xpos = -0.00125
ypos = -0.00125
zpos = 0.0
delta_x = 0.0025
delta_y = 0.0025
delta_z = 0.000304

for ik in range(1000,1600000,1000):
    #read data initialize array every time

    ts = 0.00000001

    b = np.loadtxt("./post_multi/dump"+str(ik)+".multi", skiprows = 9)
    #count particles on surface still (7 particles per bacterium)
    particle_count =
int(slice(xpos,ypos,zpos,delta_x,delta_y,delta_z,b)/float(particles_per_ba
ct))
    #Newtons
    force_amount = ik*ts*linear_force_displacement
    data.append([force_amount,particle_count])

data = np.array(data)
#print(data[:,0])
plt.plot(data[:,0],data[:,1])
#plt.show()
plt.savefig('data.png')
np.savetxt('data_summary_bacteria.csv', data, delimiter=',')

```

## MONTE CARLO SIMULATION PYTHON CODE

```

import numpy as np
import scipy as sp
import scipy.stats
import matplotlib.pyplot as plt

class Bacteria:
    def __init__(self,rho,volume):
        self.rho = rho
        self.volume = volume
        self.attached = 1

    def mass(self):
        return self.rho*self.volume

    def contact_area(self):
        #Area
        return 0.4795e-12

    def pull_off_force(self,W):
        return self.contact_area()*W

```

```

def centrifugal_force(self,omega,r_cent):
    #RCF is in g ( *9.81), omega is RPM
    #return 0.000001118*self.mass()*r_cent*omega**2*9.81
    return self.mass()*1e3*r_cent*1e-2*(omega*0.1047197551)**2
# 1 RPM = 0.1047197551 rads/s

#Initialization

#Create X amount of bacteria each with size, mass
Number_cells = int(10**(4.38))
#Number_cells = int(100)

#From First Part
[estimated_mu_rho, estimated_sigma_rho] = [0.344057242849, 0.433233356668]
#(pg/um^3)

[estimated_mu_v, estimated_sigma_v] = [3.14740477978, 0.411708258523]
#(um^3)
b = np.ndarray((Number_cells,), dtype=np.object)

for i in range(0,Number_cells):
    rand_rho = sp.stats.lognorm.rvs(estimated_sigma_rho,loc=0,scale =
estimated_mu_rho,size=1)
    rand_v = sp.stats.lognorm.rvs(estimated_sigma_v,loc=0,scale =
estimated_mu_v,size=1)
    b[i] = Bacteria(rand_rho,rand_v)

mc_steps = 100
#RPM
omega_final = 12000
W_init = 500000

def mc_simulation(mc_steps,omega_final,W_init):
    detached = 0
    j = 0

    omega_range = range(0,omega_final,mc_steps)
    percent_attached = np.zeros((len(omega_range),2))

    for omega in omega_range:
        detached = 0

        for i in range(0,Number_cells):
            if
(b[i].centrifugal_force(omega,10.7)>b[i].pull_off_force(W_init)):
                b[i].attached = 0
                detached += 1
            else:
                u = np.random.uniform(0.0,1.0)
                if(u < np.exp(b[i].centrifugal_force(omega,10.7)-
b[i].pull_off_force(W_init))):
                    b[i].attached = 0

```

```

        detached += 1
    else:
        b[i].attached = 1
    percent_attached[j]= (omega, Number_cells - detached)
    j += 1
return percent_attached

def chi(data_obs,data_model):
    yobs = data_obs[:,1]
    ymodel = data_model[:,1]
    return sum(yobs-ymodel)**2

#data input
yobs = np.genfromtxt('data_centrifuge.csv', delimiter=',')
yobs[0,0] = 0

pc2= mc_simulation(mc_steps,omega_final,10000)
pc2 =
np.array([[0,pc2[0,1]], [0,pc2[0,1]], [0,pc2[0,1]], [0,pc2[0,1]], [300,pc2[int
(300/mc_steps),1]], [300,pc2[int(300/mc_steps),1]], [1000,pc2[int(1000/mc_st
eps),1]], [1000,pc2[int(1000/mc_steps),1]], [1000,pc2[int(1000/mc_steps),1]]
, [1000,pc2[int(1000/mc_steps),1]], [4000,pc2[int(4000/mc_steps),1]], [4000,p
c2[int(4000/mc_steps),1]], [5000,pc2[int(5000/mc_steps),1]], [5000,pc2[int(5
000/mc_steps),1]], [5000,pc2[int(5000/mc_steps),1]], [5000,pc2[int(5000/mc_s
teps),1]], [10000,pc2[int(10000/mc_steps),1]], [10000,pc2[int(10000/mc_step
s),1]]])

var = 150
mc = 100
theta_init = 10000
thetal = theta_init

#Experimental Data
pc1= yobs
#Initial y_model

thetasave = np.zeros(mc)
chisave = np.zeros(mc)
for n in range(0,mc):
    theta2 = thetal + var*np.random.randn(1)

    pc2 = mc_simulation(mc_steps,omega_final,theta2)
    pc2 =
np.array([[0,pc2[0,1]], [0,pc2[0,1]], [0,pc2[0,1]], [0,pc2[0,1]], [300,pc2[int
(300/mc_steps),1]], [300,pc2[int(300/mc_steps),1]], [1000,pc2[int(1000/mc_st
eps),1]], [1000,pc2[int(1000/mc_steps),1]], [1000,pc2[int(1000/mc_steps),1]]
, [1000,pc2[int(1000/mc_steps),1]], [4000,pc2[int(4000/mc_steps),1]], [4000,p
c2[int(4000/mc_steps),1]], [5000,pc2[int(5000/mc_steps),1]], [5000,pc2[int(5
000/mc_steps),1]], [5000,pc2[int(5000/mc_steps),1]], [5000,pc2[int(5000/mc_s
teps),1]], [10000,pc2[int(10000/mc_steps),1]], [10000,pc2[int(10000/mc_step
s),1]]])

```

```
chi2 = chi(pc2,pc1)

ratio = np.exp((-chi2+chi1)/2)
u = np.random.uniform(0.0,1.0)
if u < ratio:
    theta1=theta2
    chi1 = chi2
thetasave[n] = theta1
chisave[n] = chi1

plt.plot(yobs[:,0],yobs[:,1],'bd')
plt.plot(pc2[:,0],pc2[:,1],'r+')
plt.show()
plt.hist(thetasave)
plt.show()
print("Theta Save",thetasave)
```

## **BIBLIOGRAPHY**

## BIBLIOGRAPHY

- Almond Board of California (2016). California Almond Industry Facts. Retrieved April, 11, 2017.  
from:[http://www.almonds.com/sites/default/files/content/attachments/2016\\_almond\\_industry\\_factsheet.pdf](http://www.almonds.com/sites/default/files/content/attachments/2016_almond_industry_factsheet.pdf)
- Agricultural Marketing Service, USDA. 7 CFR Part 981. March 30, 2007.
- Amberger, Stefan & Friedl, Michael & Goniva, Christoph & Pirker, Stefan & Kloss, Christoph. (2012). Approximation of Objects by Spheres for Multisphere Simulations in DEM. ECCOMAS 2012 - European Congress on Computational Methods in Applied Sciences and Engineering, e-Book Full Papers.
- Araújo, E. A., Andrade, N. J. d., Silva, L. H. M. d., Carvalho, A. F. d., Silva, C. A. d. S., & Ramos, A. M. (2009). Control of microbial adhesion as a strategy for food and bioprocess technology. *Food Bioprocess Technologies*, 3(3), 321-332.
- Arminger, G., & Muthén, B. O. (1998). A Bayesian approach to nonlinear latent variable models using the Gibbs sampler and the Metropolis-Hastings algorithm. *Psychometrika*, 63(3), 271-300.
- Banga, J. R., Balsa-Canto, E., Moles, C. G., & Alonso, A. A. (2003). Improving food processing using modern optimization methods. *Trends in Food Science & Technology*, 14(4), 131-144. doi: [http://doi.org/10.1016/S0924-2244\(03\)00048-7](http://doi.org/10.1016/S0924-2244(03)00048-7).
- Benoit, A. (2013). Experimental and mathematical models for *Listeria Monocytogenes* transfer between delicatessen meats and contact surfaces (Master's thesis). Retrieved from Proquest Dissertations and Theses database, Ann Arbor, MI.
- Beuchat, L. R., & Mann, D. A. (2014). Survival of Salmonella on dried fruits and in aqueous dried fruit homogenates as affected by temperature. *Journal of Food Protection*, 77(7), 1102-1109.
- Bowen, W. R., Lovitt, R. W., & Wright, C. J. (2001). Atomic force microscopy study of the adhesion of *Saccharomyces cerevisiae*. *Journal of Colloid and Interface Science*, 237(1), 54-61. doi: <http://dx.doi.org/10.1006/jcis.2001.7437>.
- Bratbak, G., & Dundas, I. (1984). Bacterial dry matter content and biomass estimations. *Applied and Environmental Microbiology*, 48(4), 755-757.
- Brown, K. L. (2000). Control of bacterial spores. *British Medical Bulletin*, 56, 158-171.
- Burnham, K. P., & Anderson, D. R. (2010). Model selection and multimodel inference: practical informatino-theoretic approach. New York, NY: Springer.

- Centers for Disease and Control, (CDC). (2016, 19 August, 2016). Estimates of Foodborne Illness in the United States Retrieved April, 11, 2017, from: <https://www.cdc.gov/foodborneburden/>
- Coldrey, E. (1943). Pasteurization of Milk. *British Medical Journal*, 1(4279), 52-52.
- Crumrine, M. H., Foltz, V. D., & Harris, J. O. (1971). Transmission of *Salmonella montevideo* in wheat by stored-product insects. *Applied Microbiology*, 22(4), 578-580.
- Danyluk, M. D., Jones, T. M., Abd, S. J., Schlitt-Dittrich, F., Jacobs, M., & Harris, L. J. (2007). Prevalence and amounts of *Salmonella* found on raw California almonds. *Journal of Food Protection*, 70(4), 820-827.
- Difco. (2009). *Manual of microbiological culture media*. Sparks, Maryland: Becton, Dickinson and Company.
- Ermis, E., Farnish, R. J., Berry, R. J., & Bradley, M. S. A. (2011). Centrifugal tester versus a novel design to measure particle adhesion strength and investigation of effect of physical characteristics (size, shape, density) of food particles on food surfaces. *Journal of Food Engineering*, 104(4), 518-524. doi: <http://doi.org/10.1016/j.jfoodeng.2011.01.008>.
- Farakos, S. M. S., Pouillot, R., Johnson, R., Spungen, J., Son, I., Anderson, N., & Doren, J. M. V. (2017). A quantitative assessment of the risk of human salmonellosis arising from the consumption of almonds in the United States: the impact of preventive treatment levels. *Journal of food protection*, 80(5), 863-878.
- Food and Drug Administration, (FDA). (2010). Food Safety Modernization Act. Retrieved April, 11, 2017, from: [www.fda.gov/FSMA](http://www.fda.gov/FSMA).
- Goniva, C., Kloss, C., Deen, N. G., Kuipers, J. A. M., & Pirker, S. (2012). Influence of rolling friction on single spout fluidized bed simulation. *Particuology*, 10(5), 582-591. doi: <http://doi.org/10.1016/j.partic.2012.05.002>.
- Grocery Manufacturers Association, (GMA), (2009). Control of Salmonella in low-moisture foods. Retrieved April, 11, 2017, from: <http://www.gmaonline.org/downloads/technical-guidance-and-tools/SalmonellaControlGuidance.pdf>
- Haiko, J., & Westerlund-Wikström, B. (2013). The role of the bacterial flagellum in adhesion and virulence. *Biology*, 2(4), 1242-1267. doi: 10.3390/biology2041242.
- Hanjra, M., & Qureshi, M. E. (2010). Global water crisis and future food security in an era of climate change.
- Harris, L. J., Lieberman, V., Mashiana, R. P., Atwill Edward, & Yang, M. (2016). Prevalence and Amounts of *Salmonella* Found on Raw California Inshell Pistachios. 79(8), 1304-1315.

- Hermansson, M. (1999). The DLVO theory in microbial adhesion. *Colloids and Surfaces B: Biointerfaces*, 14(1–4), 105-119. doi: [http://dx.doi.org/10.1016/S0927-7765\(99\)00029-6](http://dx.doi.org/10.1016/S0927-7765(99)00029-6).
- Hori, K., & Matsumoto, S. (2010). Bacterial adhesion: From mechanism to control. *Biochemical Engineering Journal*, 48(3), 424-434. doi: <http://dx.doi.org/10.1016/j.bej.2009.11.014>.
- Huang, Q., Wu, H., Cai, P., Fein, J. B., & Chen, W. (2015). Atomic force microscopy measurements of bacterial adhesion and biofilm formation onto clay-sized particles. [Article]. *Scientific Reports*, 5, 16857. doi: 10.1038/srep16857.
- Isaacs, S., Aramini, J., Ciebin, B., Farrar, J. A., Ahmed, R., Middleton, D., .Ellis, A. (2005). An international outbreak of asalmoneellosis associated with raw almonds contaminated with a rare phage type of *Salmonella* Enteritidis. *Journal of Food Protection*, 68(1), 191-198. doi: 10.4315/0362-028X-68.1.191.
- Israelachvili, J. N. (2011). *Intermolecular and Surface Forces* (3rd ed.). San Diego, California: Academic Press.
- Johnson, K., Kendall, K., & Roberts, A. D. (1971). Surface energy and the contact of elastic solids. *Proceedings of the Royal Society of London*, Vol. 324, (No. 1558), pp. 301-313.
- Kalmokoff, M. L., Austin, J. W., Wan, X. D., Sanders, G., Banerjee, S., & Farber, J. M. (2001). Adsorption, attachment and biofilm formation among isolates of *Listeria monocytogenes* using model conditions. *Journal of Applied Microbiology*, 91(4), 725-734. doi: 10.1046/j.1365-2672.2001.01419.
- Kloss, C., Goniva, C., Hager, A., Amberger, S., & Pirker, S. (2012). Models, algorithms and validation for opensource DEM and CFD-DEM. *Progress in Computational Fluid Dynamics*, 12(2-3), 140-152.
- Kwakwa, A. (2006). Irradiation treatment of nuts. In A. Prakash (Ed.). *Food irradiation research and technology*: Blackwell Publishing, Ames, Iowa, USA.
- Kwapinska, M., Saage, G., & Tsotsas, E. (2006). Mixing of particles in rotary drums: A comparison of discrete element simulations with experimental results and penetration models for thermal processes. *Powder Technology*, 161(1), 69-78. doi: <http://dx.doi.org/10.1016/j.powtec.2005.08.038>
- Lambertini, E., Danyluk, M. D., Schaffner, D. W., Winter, C. K., & Harris, L. J. (2012). Risk of salmonellosis from consumption of almonds in the North American market. *Food Research International*, 45(2), 1166-1174. doi: <http://doi.org/10.1016/j.foodres.2011.05.039>
- Nguyen, V. D., Benhabib, K., Marie, C., & Coorevits, P. (2012). Heat transfer in a granular media modeled by a coupled DEM-Finite Difference Method: application to fluidized bed processes. *Procedia Engineering*, 42(0), 824-832. doi: <http://dx.doi.org/10.1016/j.proeng.2012.07.475>

- Pérez-Rodríguez, F., Valero, A., Todd, E. C. D., Carrasco, E., García-Gimeno, R. M., & Zurera, G. (2007). Modeling transfer of *Escherichia coli* O157:H7 and *Staphylococcus aureus* during slicing of a cooked meat product. *Meat Science*, 76(4), 692-699. doi: <http://dx.doi.org/10.1016/j.meatsci.2007.02.011>
- Razatos, A., Ong, Y.-L., Sharma, M. M., & Georgiou, G. (1998). Molecular determinants of bacterial adhesion monitored by atomic force microscopy. *Proceedings of the National Academy of Sciences*, 95(19), 11059-11064.
- Rijnaarts, H. H. M., Norde, W., Bouwer, E. J., Lyklema, J., & Zehnder, A. J. B. (1995). Reversibility and mechanism of bacterial adhesion. *Colloids and Surfaces B: Biointerfaces*, 4(1), 5-22. doi: [http://dx.doi.org/10.1016/0927-7765\(94\)01146-V](http://dx.doi.org/10.1016/0927-7765(94)01146-V)
- Schneider, C. A., Rasband, W. S., & Eliceiri, K. W. ((2012)). NIH Image to ImageJ: 25 years of image analysis. *Nature Methods*, 9, 671-675.
- Scallan, E., Hoekstra, R. M., Angulo, F. J., Tauxe, R. V., Widdowson, M.-A., Roy, S. L., . . . Griffin, P. M. (2011). Foodborne illness acquired in the United States—major pathogens. *Emerging infectious diseases*, 17(1), 7.
- Shapiro, S. S. and Wilk, M. B. (1965). "Analysis of variance test for normality (complete samples)", *Biometrika* 52: 591–611.
- Sheen, S., & Hwang, C.-A. (2010). Mathematical modeling the cross-contamination of *Escherichia coli* O157:H7 on the surface of ready-to-eat meat product while slicing. *Food Microbiology*, 27(1), 37-43. doi: <http://doi.org/10.1016/j.fm.2009.07.016>
- United States Department of Agriculture, (USDA). (2001). USDA Guidelines for the sanitary design and fabrication of dairy processing equipment. Washington, DC: U.S. Department of Agriculture. Retrieved April, 20, 2017, from: <https://www.ams.usda.gov/>
- You, S., & Wan, M. P. (2014). Modeling and experiments of the adhesion force distribution between particles and a surface. *Langmuir*, 30(23), 6808-6818. doi: 10.1021/la500360f